The Geological Society of America
Special Paper 436
2007

New constraints on the sedimentation and uplift history of the Andaman-Nicobar accretionary prism, South Andaman Island

R. Allen
Department of Environmental Science, Lancaster University LA1 4YQ, UK

A. Carter
Research School of Earth Sciences, Birkbeck and University College London, Gower St., London WC1E 6BT, UK

Y. Najman
Department of Environmental Science, Lancaster University LA1 4YQ, UK

P.C. Bandopadhyay
Geological Survey of India, Geodata Division, Salt Lake, Kolkata, 91, India

H.J. Chapman
M.J. Bickle
Department of Earth Sciences, Cambridge University, Downing St., Cambridge CB2 3EQ, UK

E. Garzanti
G. Vezzoli
S. Andò
Dipartimento di Scienze Geologiche e Geotecnologie, Universita Milano-Bicocca, Piazza della Scienza 4, 20126 Milano, Italy

G.L. Foster
Department of Earth Sciences, Bristol University, Queens Rd., Bristol BS8 1RJ, UK

C. Gerring
Department of Earth Sciences, The Open University, Walton Hall, Milton Keynes MK7 6AA, UK

ABSTRACT

The Andaman Islands are part of the Andaman-Nicobar Ridge; an accretionary complex that forms part of the outer-arc ridge of the Sunda subduction zone. The Tertiary rocks exposed on the Andaman Islands preserve a record of the tectonic evolution of the surrounding region, including the evolution and closure of the Tethys Ocean. Some of the Paleogene sediments on Andaman may represent an offscraped part of the early Bengal Fan. Through field and petrographic observations, and use of a number of isotopic tracers, new age and provenance constraints are placed on the

Allen, R., Carter, A., Najman, Y., Bandopadhyay, P.C., Chapman, H.J., Bickle, M.J., Garzanti, E., Vezzoli, G., Andò, S., Foster, G.L., and Gerring, C., 2007, New constraints on the sedimentation and uplift history of the Andaman-Nicobar accretionary prism, South Andaman Island, *in* Draut, A., Clift, P.D., and Scholl, D.W., eds., Formation and Applications of the Sedimentary Record in Arc Collision Zones: Geological Society of America Special Paper 436, p. XXX–XXX, doi: 10.1130/2007.2436(11).

key Paleogene formations exposed on South Andaman. A paucity of biostratigraphic data poorly define sediment depositional ages. Constraints on timing of deposition obtained by dating detrital minerals for the Mithakhari Group indicate sedimentation after 60 Ma, possibly younger than 40 Ma. A better constraint is obtained for the Andaman Flysch Formation, which was deposited between 30 and 20 Ma, based on Ar-Ar ages of the youngest detrital muscovites at ca. 30 Ma and thermal history modeling of apatite fission-track and U-Th/He data. The latter record sediment burial and inversion (uplift) at ca. 20 Ma. In terms of sediment sources the Mithakhari Group shows a predominantly arc-derived composition, with a very subordinate contribution from the continental margin to the east of the arc. The Oligocene Andaman Flysch at Corbyn's Cove is dominated by recycled orogenic sources, but it also contains a subordinate arc-derived contribution. It is likely that the sources of the Andaman Flysch included rocks from Myanmar affected by India-Asia collision. Any contribution of material from the nascent Himalayas must have been minor. Nd isotope data discount any major input from cratonic Greater India sources.

Keywords: Andaman, accretionary wedge, arc, subduction, thermochronology, provenance, uplift.

INTRODUCTION

The Andaman-Nicobar Islands are part of an accretionary complex that forms the outer arc ridge of the northern Sunda subduction zone (Fig. 1). The Andaman Islands are in the southeastern part of the Bay of Bengal and make up part of a 3000–5000 km chain that runs from the Myanmar Arakan-Yoma down to Sumatra and Java in the south. The Indian plate is subducting northward below the Euarasian plate and obliquely below the Sino-Burman plate along the Burma-Andaman-Java Trench. The structure of the Andaman Islands comprises an accretionary prism formed by an imbricate stack of east-dipping fault slices and folds that young to the west (Fig. 2), linked to a westward-shifting subduction zone (e.g., Roy, 1992; Pal et al., 2003). The geology of an accretionary wedge is complex, reflecting its dynamic environments and involving subduction, folding, and thrusting. Depositional ages and environments can change abruptly over relatively short distances, and uplift leads to recycling of sediment from the eroding wedge. Throughout subduction, new material introduced at the bottom of the accretionary wedge is accreted, uplifted, or subducted. Some of the accreted material may be uplifted and brought to the seafloor. Slope basins may develop behind folds in the accreted sedimentary rocks and trap sediment in a deep-water environment. Simultaneously, shallow-water sediments such as reefs can form on the prism top and be eroded and transported down the slope. Given this inherent complexity, many accretionary complex rocks are referred to as *mélange;* thus unraveling the sedimentation history in a subduction-accretionary setting is a major task.

Interpretation of the geology of the Andaman Islands is hindered by the lack of isotopic age constraints, limited biostratigraphy, and poor outcrop exposure (Bandopadhyay and Ghosh, 1999, Bandopadhyay, 2005; Pal et al., 2003, 2005). The aim of this paper is to build on previous field-based studies and apply petrologic, isotopic, and thermochronometric techniques to better understand the provenance, sediment deposition, and uplift history.

The origin of the Andaman Flysch has been debated for >20 yr. It has been variously proposed that the Andaman Flysch was derived from the Irrawaddy Delta (Karunakaran et al., 1968; Pal et al., 2003) or, alternatively, from Bengal Fan material shed from the nascent Himalaya sourced either directly or by emplacement as an allochthon into the accretionary prism by oblique subduction (Curray et al., 1979; Curray, 2005). We are particularly interested to determine whether the Himalayan-Tibetan orogen contributed sediment to the Andaman Islands, because this might reveal information on the early evolution of the orogen not preserved elsewhere.

LITHOLOGIES

Previous Work

The current stratigraphy (Table 1) of the Andaman Islands is based on lithological mapping and can be traced back to the pioneering work of Oldham (1885), who first divided the Andaman geology into an older Port Blair Series and a younger Archipelago Series, separated by volcanic rocks and serpentinites later recognized as an ophiolite. Over the past 50 yr the stratigraphy has been modified and formation names changed, but it was not until the 1960s that paleontological constraints were used to place the Paleogene–Neogene lithostratigraphic units within a temporal framework (Guha and Mohan, 1965; Karunakaran et al., 1968). The stratigraphy now comprises four units, which, in ascending order, are Cretaceous sedimentary rocks and ophiolite, the Eocene Baratang-Mithakhari Group,

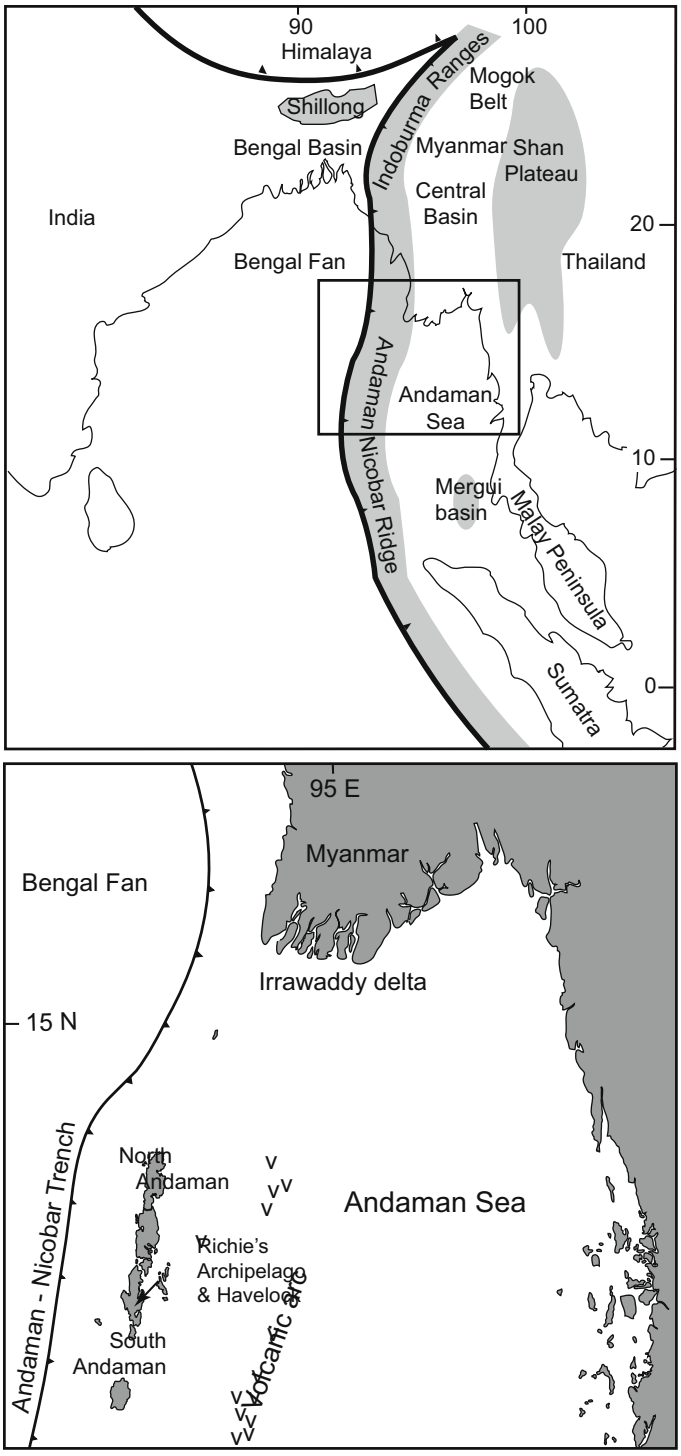

Figure 1. General location map of Andaman Islands and location of potential source regions. Lower figure corresponds to boxed area in top figure.

the Eocene to upper Oligocene Port Blair–Andaman Flysch Group, and the lower to upper Miocene Archipelago Group. In the mid-1970s the Indian state Oil and Natural Gas Commission (ONGC) carried out a detailed seismic reflection study across the Andaman Islands, calibrated against offshore boreholes drilled to the east and west of the islands (Fig. 2) that helped place the exposed geology within the context of the accretionary setting. Below we briefly describe the main rock units exposed on the Andaman Islands and report key observations from previous field and petrographic studies.

Ophiolite

The Andaman ophiolite contains the main components of an ophiolite sequence that includes upper mantle–depleted harzburgites and dunites, lower crustal cumulate gabbros and peridotites, and upper crustal sheeted dikes, pillow lavas, and marine pelagic sediments (Halder, 1985; Ray et al., 1988; Roy, 1992). However, the sequence is tectonically disturbed, and much of the crustal section is deformed and difficult to identify in the field. Pillow lavas are abundant, but sheeted dikes have been identified only in disrupted small-scale faulting and folding. Both massive and layered gabbros are recognized in the preserved ophiolite. South Andaman has the best preserved and most complete sequence of ophiolite, which extends for ~30 km from Corbyn's Cove in the north to Chiriyatapu in the south (Fig. 3).

Pelagic Sedimentary Rocks

The topmost part of the ophiolite complex contains thin and discontinuous lenses and streaks, and laterally continuous (at outcrop scale) bedded sequences of pelagic sedimentary rocks consisting of jasper, chert, cherty limestone, and shales (Bandopadhyay and Ghosh, 1999). Outcrops commonly show evidence of significant deformation and folding (Fig. 4).

Bedded Chert

Rhythmic alternations of centimeter-thick, milky white chert and millimeter- to centimeter-thick reddish-brown and purple shale-mudstone beds constitute the bedded chert facies. Chert and shale normally show uniform (0.5–4.0-cm-thick) beds that have sharp bases and tops and planar contacts. Some 10–15-cm-thick beds, and massive beds, of chert are present. Soft-sediment deformation is evident in some localities. Radiolarians are preserved to varying degrees in most cherts and indicate a Late Cretaceous to Paleocene depositional age, which constrains the underlying ophiolite sequence to a Late Cretaceous age.

Shale

At outcrop the shale facies form interbedded sequences of extremely variable thickness and lateral continuity. Basaltic volcanic rocks occur as thin intercalations, conformable lenses, and, at places, small crosscutting dikes. Thin beds of fine-grained sandstone, siltstone, and cherty limestone are also present. There is evidence of soft-sediment deformation and slump folds as well as cutting by normal and thrust faults. Some shales are clearly tuffaceous with plagioclase phenocrysts, vitric fragments, pumice clasts, and diagenetically altered volcanic lithic fragments. Chlorite is abundant in the matrix of the altered tuff and tuffaceous shale. Occasionally sharp edged, cuspate or platy, fresh glass shards can be found (Bandopadhyay and Ghosh, 1999).

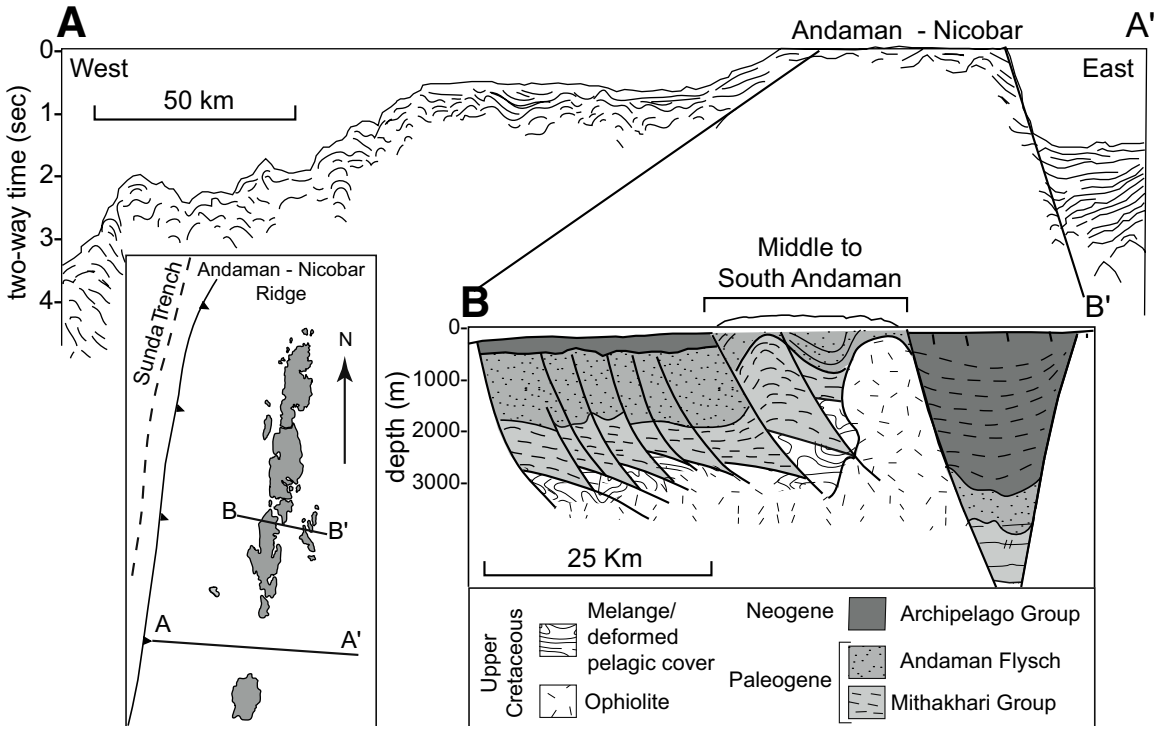

Figure 2. Cross section through Andaman Ridge, based on seismic sections from Roy (1992) and Curray (2005) that show the underlying structure of the accretionary wedge, comprising a series of folded east-dipping thrust slices.

TABLE 1. SIMPLIFIED STRATIGRAPHY OF THE ANDAMAN ISLANDS

Approximate depositional age range	Group	Formation	Lithology
Miocene to Pliocene	Archipelago Group		Cross-stratified and graded sandstones, silty mudstones and limestones marls, and chalky limestones
Oligocene–late Eocene(?)	Andaman Flysch Group (*formerly Port Blair Group*)		Bouma sequences, sandstone-shale and mudstones
Early to middle Eocene(?)	Mithakhari Group *(formerly Baratang and Port Meadow Groups)*	Namunagarh Grit	Pebbly and coarse to fine-grained volcaniclastic sandstones and grits
		Hope Town Conglomerate	Interstratified massive and graded polymict conglomerates, massive cross-stratified and graded sandstones, shales, and thin coals
		Lipa Black Shale	Pyritiferous black shale
Late Cretaceous to Paleocene(?)	Ophiolite Group		Pillow lava, basalt, gabbro, pyroxinite, harzburgite, serpentinite, andesite, diorite, plagiogranite, rhyolite, serpentinized harzburgite, pyroxinite, and pelagic sediments; radiolarian chert and hematitic mudstones

Mithakhari Group

The Mithakhari Group consists of immature gravels and coarse- to fine-grained sandstones, pebbly to fine-grained pyroclastic sandstones, and minor thin beds of mudstones and coal. Whereas the Mithakhari Group dominates the outcrop geology of the Andaman Islands, particularly in North and Middle Andaman, a paucity of good exposures and poor access make it difficult to obtain continuous sections, and exposures are limited to isolated stone quarries, coastal areas, and road cuts. In South Andaman the Mithakhari Group occurs as a north-south–trending outcrop that extends for ~50 km, but the best sections, exposing the least weathered outcrops, are found only near Hope Town, Mungleton, Namunagarh, and Chiriyatapu (Fig. 3). Karunakaran et al. (1968)

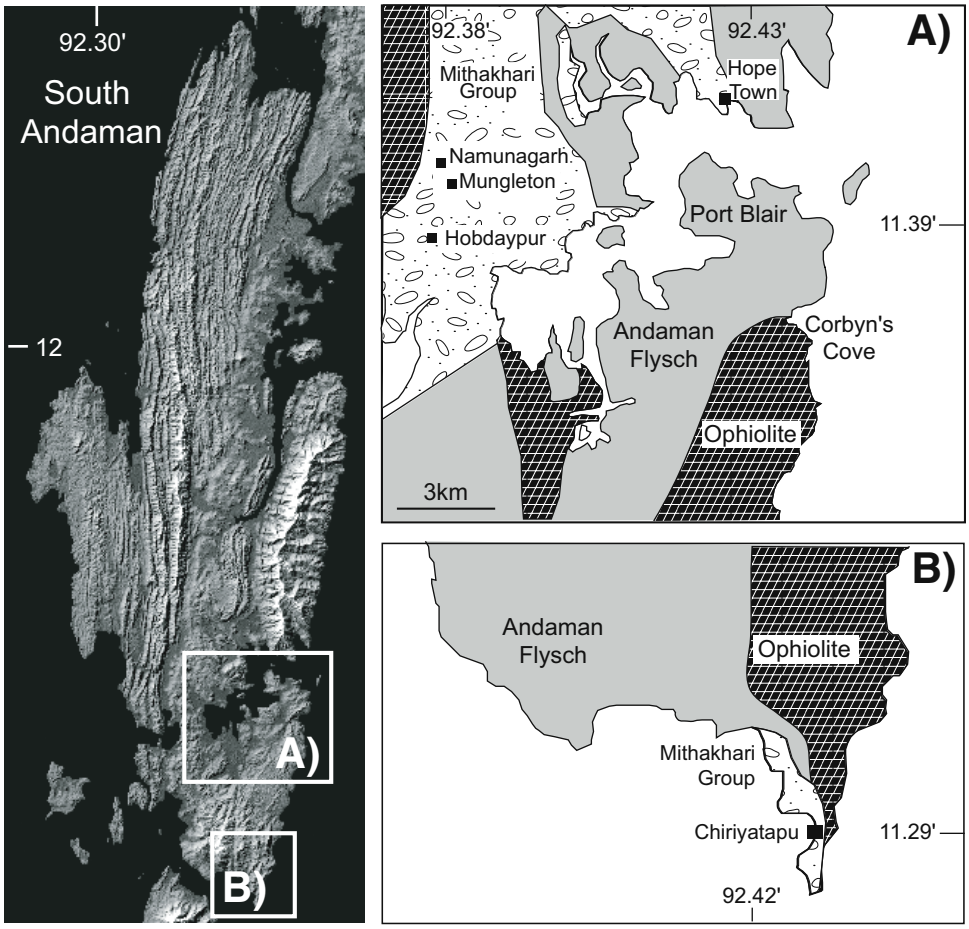

Figure 3. General location map of Andaman Islands and local geology (A, B) for the areas on South Andaman Island sampled for this study.

Figure 4. Folded cherts and shales that represent the pelagic cover to the Cretaceous ophiolite exposed on the shore at Chiriyatapu, South Andaman Island.

first introduced the term *Mithakhari Group,* dividing the group into a lower Lipa Black Shale, a middle Hope Town Conglomerate, and an upper Namunagarh Grit Formation (Table 1). The Lipa Black Shale is a minor unit and not well exposed, and so will not be considered further.

Hope Town Conglomerates

This unit is best seen near Hope Town on South Andaman Island, where ~6 m of conglomerates and pebbly sandstones are well exposed (Fig. 5), interbedded with thin beds of greenish gray coarse- and fine-grained sandstones. The sequence shows fining- and thinning-upward sequences with evidence of slumping and soft sediment deformation. Bed contacts are generally sharp and planar, and some evidence of fluvial channels can be found. Conglomerates are polymict, of mainly basic-ultrabasic sources, and with subordinate to minor amounts of andesite, sedimentary limestone, and cherts plus sporadic mudstone clasts and metamorphic quartz.

Namunagarh Grit Formation

This unit is characterized by coarse- to fine-grained sandstones and siltstone, with minor conglomerate at the base. On South Andaman the type section and best exposures are found in quarry sections near Namunagarh village (Fig. 3). These display 3–5-m-thick, green, matrix-supported sandstones. The sandstones are well bedded and laterally persistent along the quarry sections, and consist of coarse- and fine-grained beds. The coarse-grained beds, at the base of the section, are ≥1 m thick, with sharp non-erosive contacts. The finer grained beds consist of 4–8-cm-thick

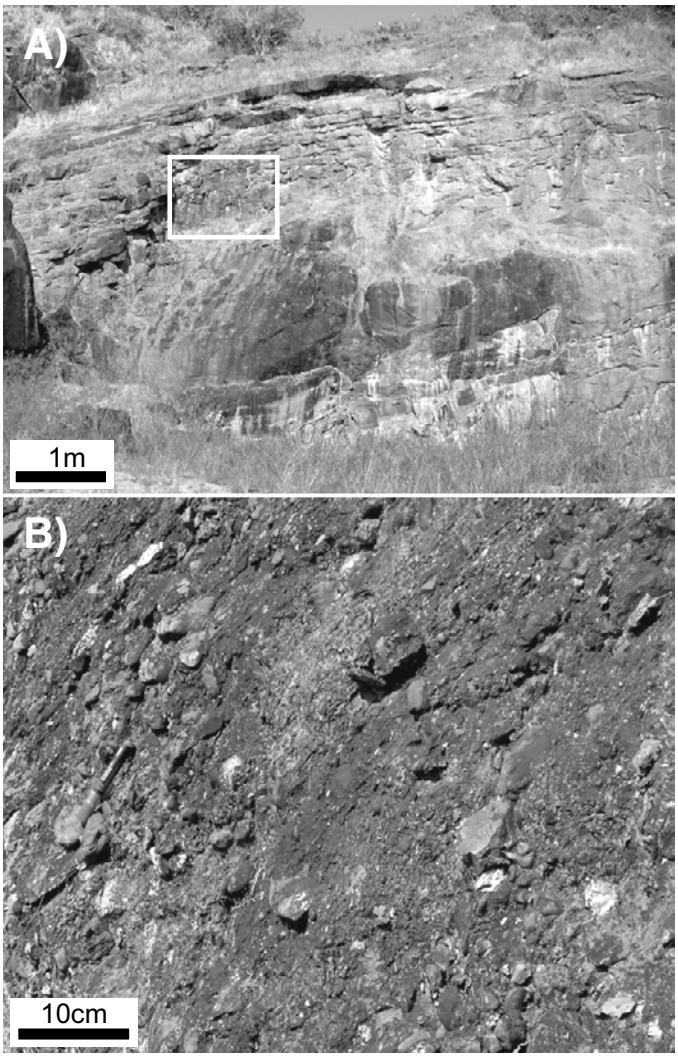

Figure 5. Massive polymict conglomerates exposed at Hope Town Quarry (A), South Andaman Island. These polymict conglomerates are dominated by basic and ophiolitic clasts (B) whereas the matrix contains abundant volcanic glass and felsitic volcanic grains, suggesting a dominant volcanic arc source, although zircon fission-track data also show evidence of continental Mesozoic sources.

beds of fine- to medium-grained volcaniclastic sandstones interbedded with thin mudstones. Some large fragments of volcanic rock fragments, including elongated pumice lapilli, are present, which resemble floating clasts in turbidites. For a long time the sandstones exposed at Namunagarh stone quarries had been described as graywacke formed from weathering and erosion of accreted ophiolite (Acharyya et al., 1989). Recently Bandopadhyay (2005) identified beds with abundant pyroclasts, including vesiculated glass fragments, pumice clasts and shards, euhedral feldspars, and angular lithic fragments diagnostic of tuff, indicating that some of the Namunagarh Grit beds were derived from direct volcanic arc sources (Fig. 6).

The polymict conglomerates (Hope Town Conglomerate) and grits (Namunagarh Grit Formation) are interpreted as having

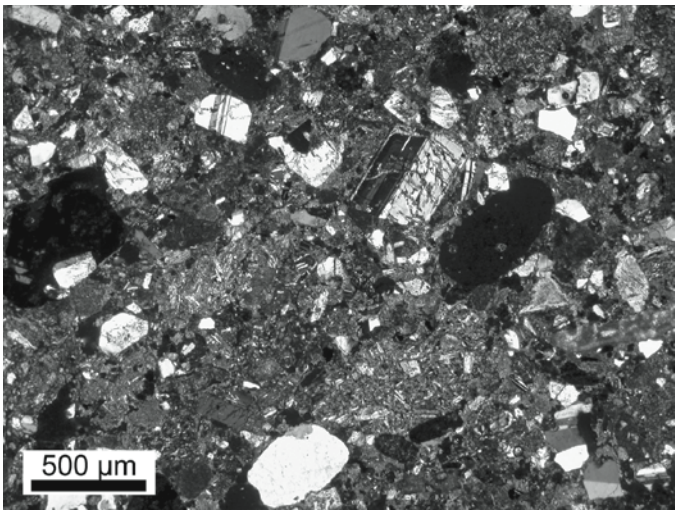

Figure 6. Namunagarh Quarry. Thin sections show that the sediments are largely tuffaceous with clear evidence of fresh arc volcanic material including devitrified glass.

been derived from the ophiolite and its pelagic–shallow marine cover. The succession, which includes thin coals and gypsum, was deposited in a delta-slope setting with facies associations ranging from subaerial alluvial plain to prodelta slope (Chakraborty et al., 1999). Its depositional age is not well defined owing to the lack of distinct biostratigraphic evidence, but shallow benthic foraminifers in the Hope Town Conglomerate, including *Nummulites atacicus*, constrain the age from late Ypresian to early Lutetian (Karunakaran et al., 1968). Many of the foraminifers, however, are broken and abraded (i.e., reworked). The relationship of the Namunagarh grits to the Hope Town conglomerates is not clear, although the Namunagarh grits are presumed to be younger.

Andaman Flysch

The Andaman Flysch is a siliciclastic turbidite sequence deposited on a submarine fan. It is bounded between the Mithakhari Group below and the Archipelago Group above. The (misleading) term *flysch* is derived from the resemblance of the turbidites to the classic Bouma turbidites described in the Swiss Alps. Similar looking beds are seen throughout the Andaman Islands; hence the Andaman Flysch is described as cropping out over a N-S strike length of 200 km from the southern part of South Andaman to the northern tip of North Andaman. The overall thickness is not well defined, with estimates varying from 750 m (Roy, 1983) to 3000 m (Pal et al., 2003). The best and most completely documented exposures are found on South Andaman at Corbyn's Cove (Fig. 3), where outcrops of steep, westerly dipping beds are seen adjacent to the pillow basalt of the ophiolite sequence (Fig. 7), although the nature of the contact is uncertain. Individual sandstone beds can be traced along strike for distances of several kilometers, but the total thickness is only 250–300 m. Current directional structures in sandstone beds

Figure 7. Outcrop of the Andaman Flysch, looking south across Corbyn's Cove (see Fig. 3) toward outcrops of pillow basalts and ophiolite.

include flute casts, groove casts, and current bedding. The orientation of flute casts at the base of overturned sandstone beds near Corbyn's Cove reveals southward-directed paleocurrents (Pal et al., 2003). The relationship between the turbidites and underlying lithostratigraphic units is unclear. Onlap of the Andaman Flysch with the Mithakhari Group has been reported (Chakraborty and Pal, 2001), but no supporting evidence was found in this study. However, there is a marked change in lithology and provenance with up to 50% quartz in the Andaman Flysch in contrast to the relatively quartz-free Mithakhari Group (Pal et al., 2003). Lithic fragments in the Andaman Flysch range from micaceous metamorphic clasts diagnostic of continental sources to cherts, basalts, and weathered volcanic glass consistent with derivation from volcanic arc and ophiolite sources. Biostratigraphic evidence is vague and spans the Oligocene to the early Miocene, ca. 36–21 Ma (Pal et al., 2003).

Archipelago Group

The Archipelago Group represents the topmost stratigraphic unit of the Tertiary succession. The lower units comprise basal conglomerates and sandstones, overlain by calcareous arenites of the Strait Formation. This is followed by chalk and limestone with some argillaceous limestones and shale, described as the Melville Limestone (Shell Limestone) Formation. Deposition was mostly in a slope environment (Pal et al., 2005; Roy, 1983). These sedimentary rocks most likely covered most of Andaman, but recent uplift and erosion means that today only small patches can be found on the main islands, with most exposures confined to Havelock Island and associated smaller islands to the east of South Andaman in Richie's Archipelago (Fig. 1). Radiolarians, planktonic foraminifers, and calcareous nannofossils from John Lawrence Island (Singh et al., 2000) indicate a maximum depositional age for the calcareous chalk in the Archipelago Group of 18.3–15.6 Ma (Burdigalian to Serravallian), but elsewhere the Archipelago Group may span any age from Miocene to Pliocene (Pal et al., 2005).

METHODOLOGICAL DETAILS

The aim of this work is to provide improved understanding of the burial and uplift history of the accretionary wedge and provenance of the constituent sedimentary rocks, now exposed on the Andaman Islands, through the application of thermochronometric, petrographic, and geochemical analyses of these rocks. Multiple proxies are used to get the best insight to the source provenance and to avoid any potential bias that might arise by relying on a single type of mineral. For example, mica is generally not present in arc-derived volcanic rocks, whereas apatite and zircon are. Sampling is confined to South Andaman, where there are accessible exposures of the main type localities, studied by Bandopadhyay and Ghosh, (1999), Chakraborty and Pal (2001), Pal et al. (2003, 2005), and Bandopadhyay (2005). Both Middle and North Andaman are less developed and thus are less accessible, with extensive areas of jungle that include large tribal reserves that are restricted to aboriginal peoples.

Samples from South Andaman were collected for detrital thermochronometric, heavy-mineral, biostratigraphic, and Sm-Nd whole rock and single grain analyses.

Zircon and Apatite Fission-Track Analysis

Apatite and zircon fission-track (FT) analyses are used to define provenance and low-temperature histories, and for places where sediments have been subjected to significant (>1.5 km) burial to determine their postdepositional burial and uplift history. Fission tracks in apatite are sensitive to relatively low temperatures (typically <60–110 °C) and are ideally suited to constrain levels of postdepositional burial and timing of subsequent rock uplift and exhumation (e.g., Green et al., 1995). Zircon FT data record higher temperature cooling histories (typically ~200–310 °C) and for sedimentary rocks are more suited to provenance studies that record either volcanic formation ages or postmetamorphic cooling-exhumation ages (Carter, 1999). Samples for FT analysis were irradiated in the well-thermalized (Cd ratio for Au >100) Hifar Reactor at Lucas Heights in Australia. Apatite grain compositions were monitored using etch pits and direct measurement on a JEOL microprobe using a defocused 15 KeV Beam to prevent F and Cl migration. Durango apatite and rock salt were used as standards. Samples with mixed ages, indicated by c^2 values <5% and large age-dispersion values (>20%), were deconvolved into their principal age components using the approach of Sambridge and Compston (1994) and incorporating the method of Galbraith and Green (1990).

Apatite Helium Analysis

Apatite helium dating was used to provide additional constraint on rock uplift histories. This method complements FT dating, as it is sensitive to closure at ~60 °C, the temperature at which FT begins to lose sensitivity to changes in cooling rate. Helium ages were based on replicate analyses of apatite grains handpicked to avoid mineral and fluid inclusions. Each selected grain was first photographed, and then its dimensions were

recorded for later alpha-ejection correction. Samples were loaded into platinum microtubes for helium outgassing and U/Th determination. Outgassing was achieved using an induction furnace at a temperature of 950 °C. The abundance of ^{4}He was measured relative to a 99.9% pure ^{3}He spike in a Pfeiffer Prisma 200 quadrupole mass spectrometer. The quantification of U/Th was performed on an Agilent 7500 quadrupole mass spectrometer using spiked solutions of the dissolved apatite. Repeated analysis of the California Institute of Technology (CIT) laboratory Durango apatite standard gives an age of 31.3 ± 1.2 Ma (2σ), based on 39 analyses. This error of the mean (6.7%), combined with the U/Th and He analytical uncertainties, is used as a measure of the total uncertainty in sample age.

Ar-Ar Age Dating of Detrital White Micas

The $^{40}Ar/^{39}Ar$ age of a detrital muscovite records the timing of cooling and exhumation (or crystallization) of rocks in the source region, aiding the discrimination of potential source regions for clastic sequences (e.g., Sherlock and Kelley, 2002; Haines et al., 2004). For this study, single grains were totally fused using an infrared laser ablation microprobe (IRLAMP). Samples were monitored using the GA1550 biotite standard with an age of 98.8 ± 0.5 Ma (Renne et al., 1998). The calculated *J* value for the samples was 0.0138 ± 0.000069. Blanks were measured both before and after each pair of sample analyses, and the mean of the two blanks was used to correct the sample analyses for the measured isotopes. Overall mean blank levels for ^{40}Ar, ^{39}Ar, and ^{36}Ar were (378, 6, and 11) × 10^{-12} cm^3 at a standard temperature and pressure. The resulting analyses were also corrected for mass spectrometer discrimination, ^{37}Ar decay, and neutron induced interferences. The correction factors used were $(^{39}Ar/^{37}Ar)_{Ca}$ = 0.00065, $(^{36}Ar/^{39}Ar)_{Ca}$ = 0.000264, and $(^{40}Ar/^{39}Ar)_{K}$ = 0.0085; these were based on analyses of Ca and K salts. Samples were irradiated for 33 h in the McMaster University reactor (Canada).

U-Pb Dating of Detrital Zircon

Zircon U-Pb dating reflects the time of zircon growth, which in most cases is the igneous rock's crystallization age. The U-Pb system is mostly unaffected by high-grade metamorphism and is effectively stable up to ~750 °C (Cherniak and Watson, 2001; Carter and Bristow, 2000). Zircon U-Pb ages from detrital grains in a sedimentary rock are therefore expected to be representative of the range of crustal ages within the contributing drainage basin. Samples for this study were analyzed at University College London by laser ablation-inductively-coupled-plasma mass spectrometry (LA-ICP-MS) using a New Wave 213 aperture imaged frequency quintupled laser ablation system (213 nm) coupled to an Agilent 750 quadrupole ICP-MS. Real-time data were processed using GLITTER and repeated measurements of the external zircon standard PL (Svojtka et al., 2001; TIMS reference age 337.1 ± 0.7 Ma) to correct for instrumental mass bias. The results have not been corrected for common lead or ranked according to degree of discordance, as the latter involves choosing an arbitrary value and is therefore open to analyzer bias.

Sm-Nd Isotope Analysis

Whole rock Sm and Nd isotope data in sedimentary rocks are widely used to fingerprint sediment source. $^{143}Nd/^{144}Nd$ ratios are generally normalized and expressed in epsilon units as deviation from a chondritic uniform reservoir (CHUR), where εNd = 0. A single epsilon unit is equivalent to a difference in the $^{143}Nd/^{144}Nd$ ratio at the 4th digit. For clastic sedimentary rocks, εNd will in part represent the weighted average of the time when the sediment sources were extracted from the mantle. When melt is extracted from the mantle, it has a lower Sm/Nd ratio than its parent and therefore evolves over time to have a lower εNd than CHUR; the residual has a higher Sm/Nd than CHUR, evolving to a higher εNd over time.

For this study, sandstone and mudstone samples were collected from type localities from the Andaman Flysch and the Mithakhari Group. Whole rock samples were ignited overnight at 900 °C to remove any organic material. Dissolution and analytical methods follow Ahmad et al. (2000), with the exception that the samples were spiked with a mixed ^{150}Nd-^{149}Sm spike and the ^{143}Nd-^{144}Nd ratios were measured on the spiked fraction. εNd is calculated relative to the present day (i.e., at t = 0) using CHUR $^{143}Nd/^{144}Nd$ = 0.512638. Sm and Nd blanks were $<10^{-3}$ of the sample, and the laboratory Johnson Mathey Nd internal standard gave $^{143}Nd/^{144}Nd$ = 0.511119 ± 5 (1σ = 24) over the period of the analyses. As whole rock εNd typically represents the weighted average of sediment sources, further insight into the origin of the Andaman Flysch was achieved by analyzing the Nd isotopic character of single apatite grains. This was achieved using a 193 nm homogenized ArF New Wave/Merchantek laser ablation system linked to a ThermoFinigan Neptune multicollector mass spectrometer at the University of Cambridge (UK). All ablation was carried out in a He environment and mixed with Ar and N after the ablation cell. Laser spot sizes were 65–90 μm. During the analytical period, standards reproduced to better than 0.5 epsilon units, while samples typically gave internal precisions of 1–2 epsilon units. The full methodology of this in situ approach is detailed in Foster and Vance (2006).

Petrography and Heavy Minerals

A total of 400 points were counted in six selected samples according to the Gazzi-Dickinson method (Dickinson, 1985). A classification scheme of grain types allowed for the collection of fully quantitative information on the sampled sandstones. Transparent dense minerals were counted on grain mounts according to the "ribbon counting" method, and 200 minerals were counted also to assess the percentage of etched and corroded grains. Dense minerals were concentrated with sodium metatungstate (density, 2.9 g/cm^3) using the 63–250 μm fraction treated with hydrogen peroxide, oxalic acid, and sodium ditionite to eliminate organic matter, iron oxides, and carbonates, respectively.

RESULTS AND INTERPRETATION

Biostratigraphy

Attempts to identify new, more robust biostratigraphic control for the Paleogene sedimentary rocks, based on nannofossils, failed owing to the barren nature of the mudstones. Samples of mudstone were taken from the Archipelago Group, Andaman Flysch Group, and the Mithakhari Group. Whereas nannofossils are present in the calcareous Neogene sedimentary rocks (Archipelago Group) (Singh et al., 2000), we can only conclude that nannofossils either were never present in the Paleogene sedimentary rocks or have since been dissolved by weathering or dissolution below the carbonate compensation depth. Similarly, the sampled rocks yield few (as yet undated) foraminifers. Those found were either broken or abraded, consistent with reworking. At Chiriyatapu, clasts of limestone were present within the coarse-grained Mithakhari sedimentary rocks (Fig. 8A). These were found to have shallow marine reef assemblages, including *Nummulites* spp., small miliolids and rare *Morozovella* spp., fragments of rhodophyte algae, and dasycladaceans (*Belzungia* spp.) of Thanetian–Ypresian age (ca. 58–49 Ma) (Fig. 8B).

Fission-Track and (U/Th)-He Thermochronometry

Samples from the Mithakhari Group contained relatively low concentrations of heavy minerals and yielded fewer apatites and zircons than those from the Andaman Flysch. For this reason, FT data sets from the Mithakhari Group were smaller in comparison with those from the Andaman Flysch. Nevertheless the results adequately provide a measure of the underlying detrital FT signatures for each key lithostratigraphic unit. Data are summarized as radial plots in Figures 9 and 10, and tabulated in Table A1 (Appendix).

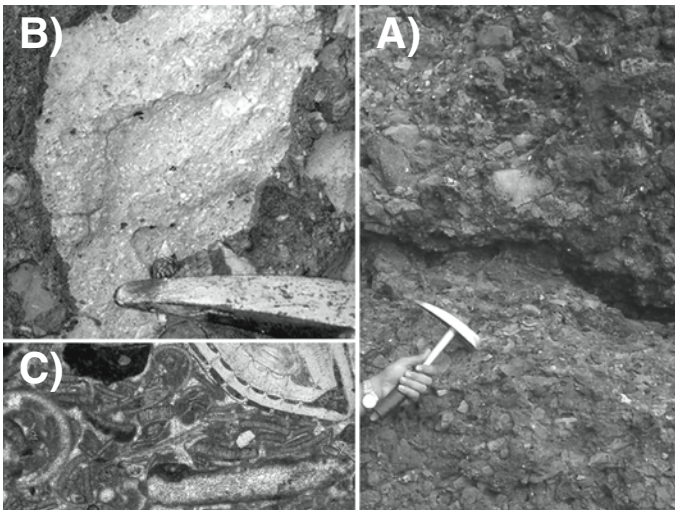

Figure 8. A and B show clasts of limestone from Mithakhari sediments. These contain shallow-marine reef assemblages that in thin section (C) are seen to include *Nummulites* spp., small miliolids and rare *Morozovella* spp., fragments of rhodophyte algae, and dasycladaceans (*Belzungia* spp.) that indicate a Thanetian–Ypresian depositional age. No in situ outcrops of these beds have been found on South Andaman.

The interpretation of detrital apatite FT data requires comparing youngest ages with sediment depositional age. If all single grain ages are less than depositional age, total resetting took place (generally indicating burial heating to >100–120 °C; e.g., Green et al., 1995, their Fig. 12), whereas if the population of measured single grain ages ranges from younger to older than depositional age, partial resetting has taken place (generally indicating burial heating to <100 °C). The main issue with interpreting the Andaman FT data is that suitable depositional ages are missing, preventing robust use of FT analysis to determine exhumation rates. Samples from the Hope Town Conglomerate collected at the Hope Town quarry (Fig. 5) yield a single population of apatites with an age of 57 ± 9 Ma. The large uncertainty in age is due to low uranium concentrations. The zircon ages comprise three age modes, with the youngest (majority of analyzed grains) at 61 ± 2 Ma, within error of the apatite age. The other zircon ages indicate sources with Late Cretaceous and Permian cooling signatures. Given that the zircon grain ages from the Hope Town Conglomerate are at or older than the Eocene biostratigraphic age (maximum age owing to the reworked nature of the fossils), the FT ages must reflect different sources. Furthermore, given that the apatite grains have the same age as the youngest zircon ages, the apatite data must also reflect provenance.

The youngest apatite and zircon ages at ca. 60 Ma constrain depositional age to being at or after this time for the Hopetown Conglomerate Formation at this location. The apatites are noticeably euhedral, contain variable chlorine, and are low in uranium (Fig. 11), typical of volcanic apatites, consistent with sample petrography that records a dominant flux of volcanic detritus (see below). Similar FT ages and volcanic affinities are seen in the apatite and zircon data from the Mungleton quarry (20 km inland from the Hope Town quarry; Fig. 5), exposing a 6-m-thick sequence of interbedded greenish-gray, fine- to medium-grained sandstones, siltstones, and mudstones, underlain by conglomerates. The succession here was described as the Namunagarh Grit Formation. In contrast, the apatite FT data from a quarry at Namunagarh village (also mapped as Namunagarh Grit Formation) gave a single population age of 40 ± 4 Ma, based on 24 grains. The zircon content of this sample was too low for FT analysis. This quarry, studied by Bandopadhyay (2005), comprises tuffaceous beds with well-preserved pumice fragments and glass shards. The apatites are euhedral and have variable chlorine and low uranium contents typical of volcanic sources. Detrital assemblages in these rocks contain pyroxenes, epidote, sphene, green-brown hornblende, and chrome spinel that are consistent with provenance from a volcanic arc. Major diagenetic dissolution is also evident, so it is questionable whether the apatite age reflects source or resetting. No track lengths were measured as

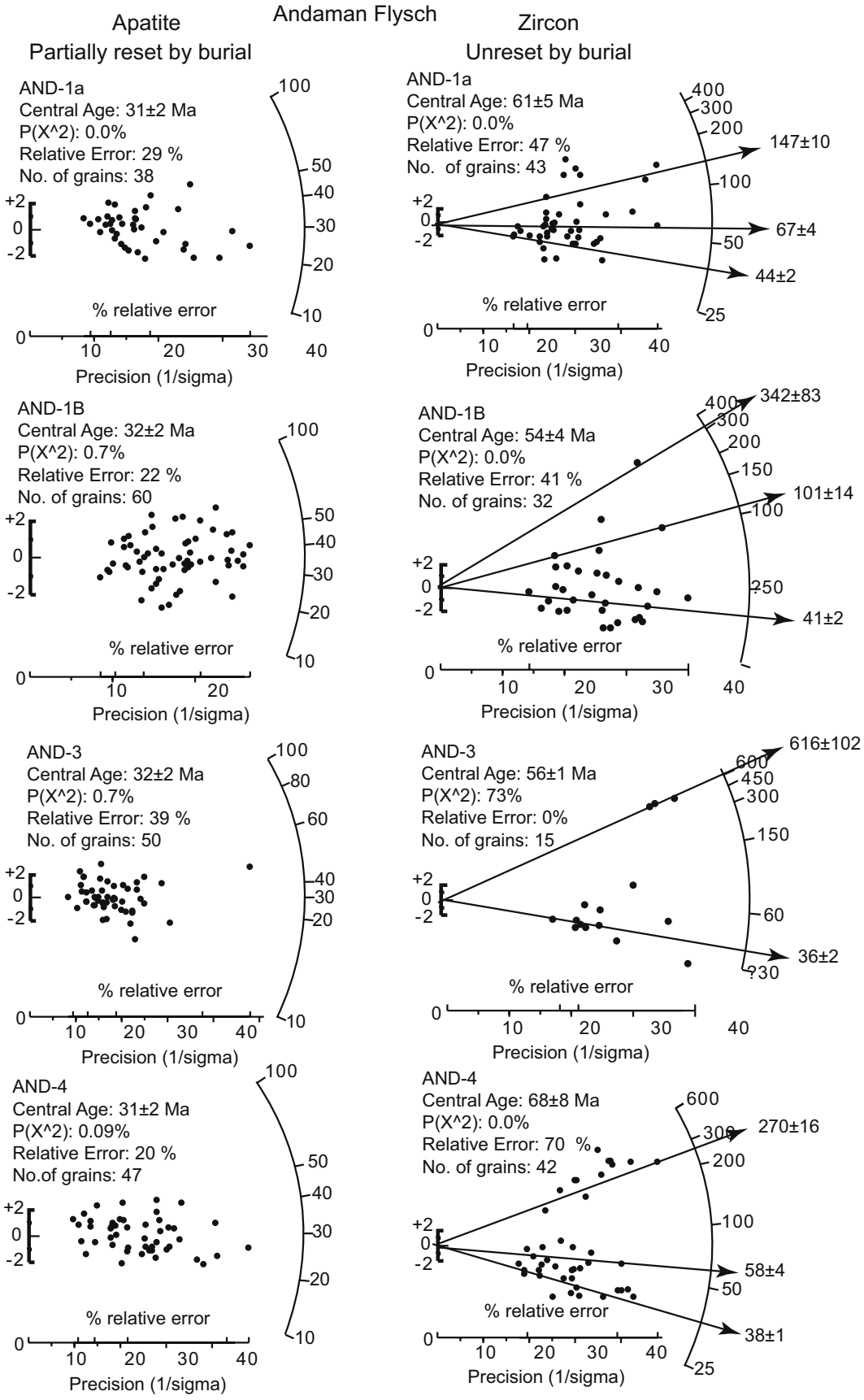

Figure 9. Radial plots of fission-track data from the Andaman Flysch, showing the distribution of single grain ages. Where the sample data comprise mixed grain ages the deconvolved age modes are also shown.

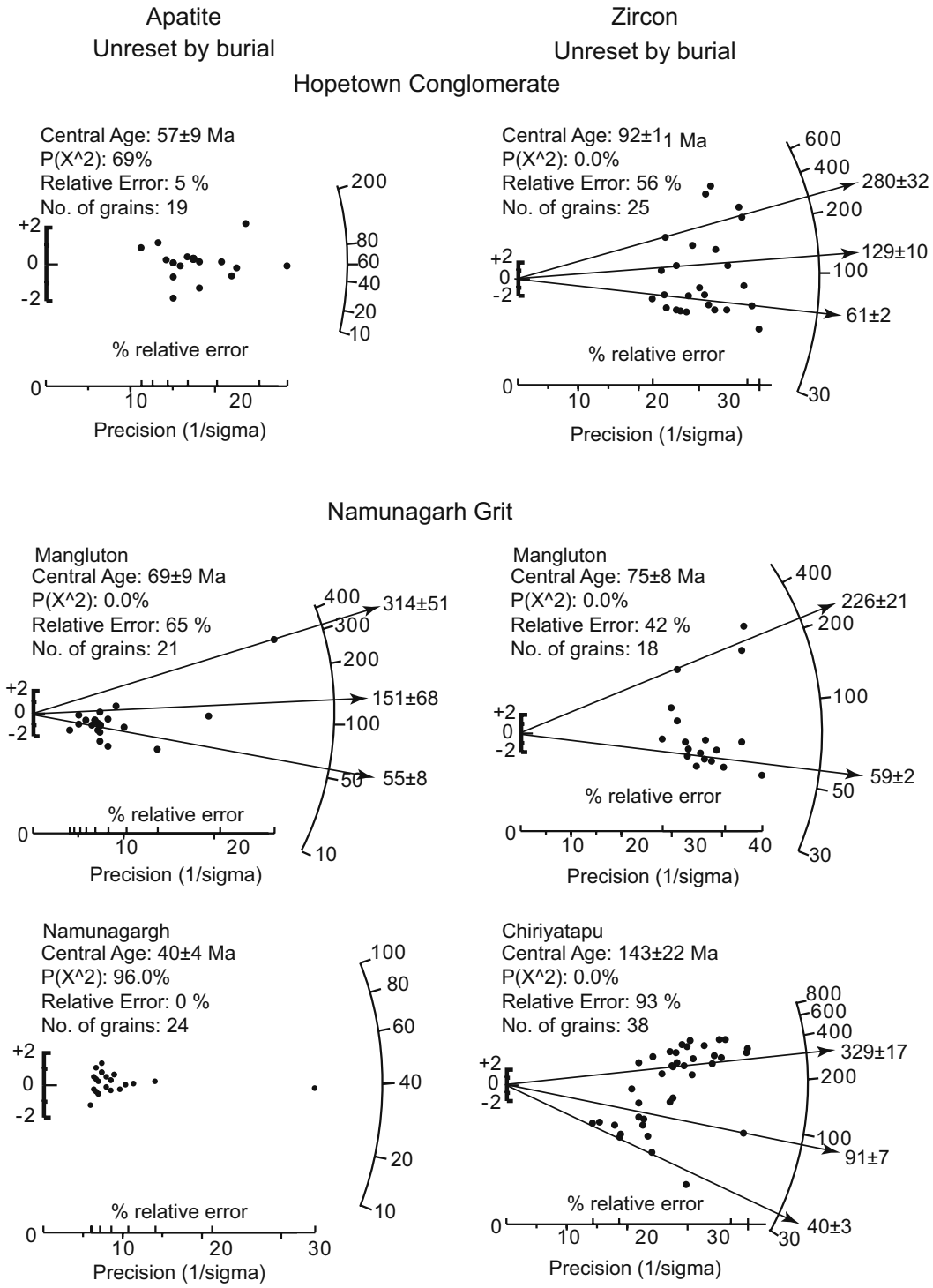

Figure 10. Radial plots of fission-track data from the Mithakhari Group, showing the distribution of single grain ages. Where the sample data comprise mixed grain ages the deconvolved age modes are also shown.

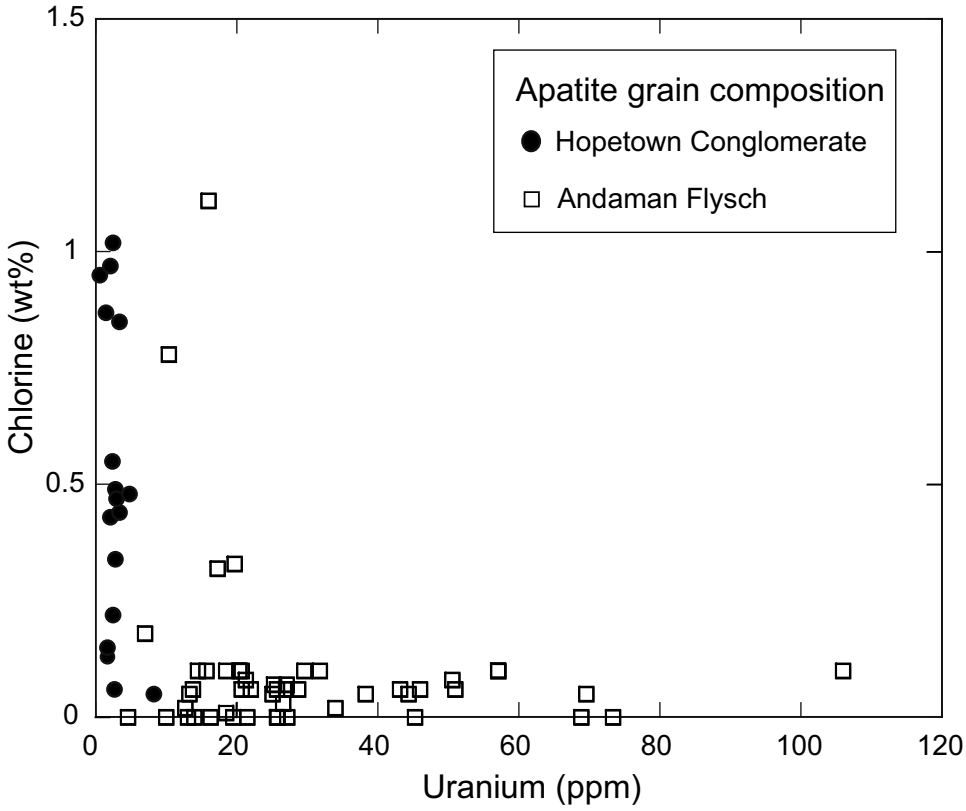

Figure 11. Plot comparing uranium and chlorine for apatite grains from the Andaman Flysch and Hopetown Conglomerate, Mithakhari Group. The plot clearly shows that the apatite came from different sources. The low uranium Hopetown Conglomerate apatites, which also have variable amounts of chlorine, are typical of volcanic apatites. The volcaniclastic petrography and euhedral form of the apatites support this and suggest that they came from arc related sources.

a result of the low spontaneous track density. A sample of the Namunagarh Grit Formation from Chiriyatapu on the southern coast of South Andaman yielded only zircon, which produced three FT provenance age modes at 40 ± 3 Ma, 91 ± 7 Ma, and 329 ± Ma. The youngest zircon FT age mode, at 40 ± 3 Ma, indicates that the Thanetian–Ypresian limestone clasts found in these rocks were derived from erosion of significantly older material (by ca. 16 Ma). Thus we conclude that the age of the Mithakhari Group is constrained to be younger than 60 Ma at two locations, and younger than 40 Ma at a third location. Nevertheless, the volcanic origin of the material, with little sign of reworking, suggests that the rocks were deposited only shortly after the mineral ages were reset. This is consistent with diachronous deposition in local basins, as expected in a subduction zone setting (e.g., Draut and Clift, 2006).

Apatite and zircon FT data from four samples collected through the section of Andaman Flysch at Corbyn's Cove are closely similar in age (most are 35–40 Ma) to the youngest age modes in the Namunagarh Grit Formation beds. The youngest ages comprise most analyzed grains for zircon and all analyzed grains for the apatites. In addition, two of the samples show zircon age modes at 58–67 Ma, similar to the age modes detected in the Mithakhari Group. Three of the samples also show Mesozoic and Paleozoic FT ages. The Andaman Flysch is widely considered to be Oligocene in age, although biostratigraphic evidence is not robust (Pal et al., 2003). While both zircon and apatite FT ages are older than the Oligocene, some partial resetting (burial-related heating) may have taken place.

Thermal Modeling

To constrain postdepositional thermal history, apatites from one of the samples were analyzed by the (U/Th)-He method (Table A2, Appendix). Replicates yielded an FT corrected age of 16 ± 1 Ma, crudely representing the time at which the sample cooled to <50 ± 10 °C. To define more robustly the sample postdepositional thermal history, the FT and helium data can be jointly modeled. Ideally this requires incorporating a sample depositional age, but, as discussed, this is not well defined, and so we resorted to using the youngest detrital ages as an upper limit for the time of deposition. For the Andaman Flysch, deposition must have taken place at or after 35–30 Ma on the basis of the youngest argon mica ages. In addition the Andaman Flysch sedimentary rocks must have been at or near surface temperatures by the middle Miocene (ca. 16 Ma) because in the Hobdaypur area of South Andaman (Fig. 2) these rocks are seen to be conformably overlain by sedimentary rocks of the Archipelago Group, although in the eastern part of the island Archipelago rocks are juxtaposed with rocks of the Mithakhari Group along a faulted contact (Pal et al., 2005). A phase of reburial up to ~60 °C

is also required on the basis of recent diagenetic evidence from the Archipelago Group sedimentary rocks (Pal et al., 2005). With these constraints the combined apatite FT and helium data were modeled, using the data-driven modeling approach of Gallagher (1995) that combines multicompositional FT annealing and helium diffusion models (Ketcham et al., 1999; Meesters and Dunai, 2002). The best-fit solution (Fig. 12) highlights three important stages: (1) a requirement for deposition and burial to peak temperatures of ~80–90 °C between ca. 30 and 25 Ma, (2) uplift to the surface between ca. 25 and 20 Ma, and (3) reburial in the Miocene (ca. 25–5 Ma) to temperatures of 50–60 °C (broadly equivalent to depths of ~1–1.5 km, assuming geothermal gradients of 30 °C/km).

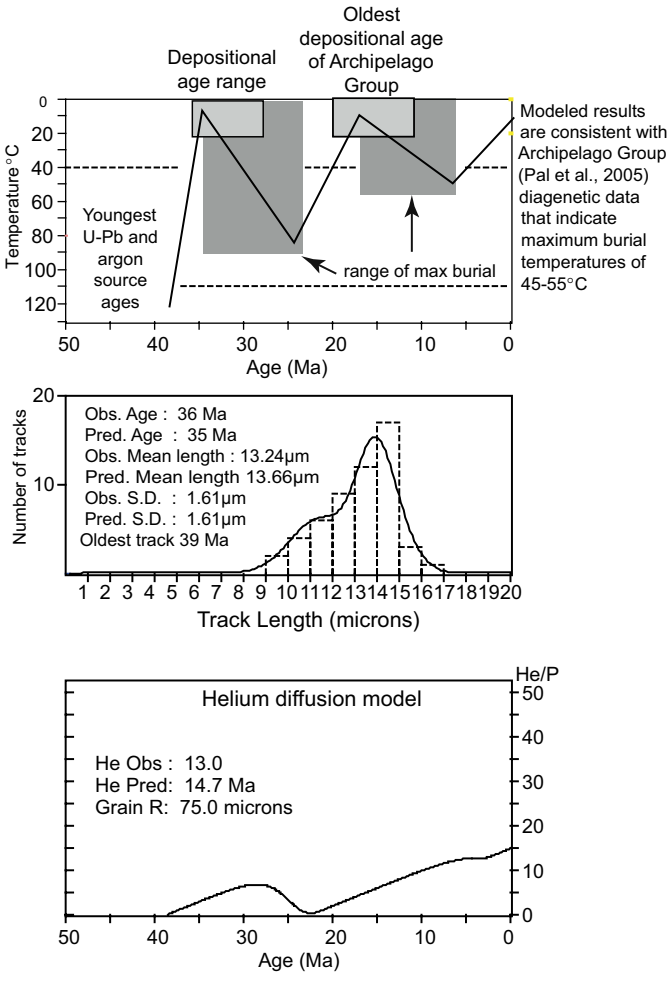

Figure 12. Best-fit thermal-history model for apatite fission-track and (U-Th)/He data from the Andaman Flysch. Key features are a requirement for maximum burial temperatures between ca. 20 and 30 Ma and rapid cooling at ca. 20 Ma. Values given are for observed data (Obs.), model predicted values (Pred.), and standard deviation (S.D.). For the helium plot, R is the grain radius and He/P is the helium concentration profile.

Detrital Argon Data

Four samples were analyzed from the Andaman Flysch, Corbyn's Cove section, which yielded 114 grain ages. One additional sample from Mithakhari Group sedimentary rock at Chiriyatapu was also analyzed (33 grain ages). The results are displayed as probability plots in Figure 13 and tabulated in Table A3 (Appendix). Ages for the Mithakhari Group sample extend from 70 Ma to the Archean, with the bulk of ages spanning the Mesozoic and Paleozoic. The Andaman Flysch ages are in general younger, ranging from 30 Ma to the Proterozoic. Most of the ages (71 grains) are <200 Ma, with 20 grains falling between 30 and 60 Ma, and 32 grains between 60 and 80 Ma. Given that postdepositional heating was modest, as constrained by the FT data, which measure lower closure temperatures than argon, the young mica ages, some of which are younger than the FT data, point to an Oligocene depositional age: i.e., the Andaman Flysch was deposited at or after 30 Ma.

Detrital Zircon U-Pb Data

Preliminary zircon U-Pb data from the Andaman Flysch (Fig. 14; Table A4, Appendix) show a large Proterozoic population, with a few grains showing Archean and Cretaceous–Eocene ages. The youngest zircons (five grains) give an average age of 48 ± 5 Ma, which overlaps both zircon FT and mica ages. These grains are euhedral and have concentric zoning typical of magmatic zircon, suggesting a direct contribution from an early Eocene igneous source rather than reworking of older sedimentary deposits.

Petrography and Heavy Mineral Data

The very fine to fine-grained turbidites of the Andaman Flysch have an intermediate quartz content (Q 49 ± 2%) (Fig. 15) and contain subequal amounts of feldspar (F 22 ± 6%; plagioclase feldspar 39 ± 9%) and lithic grains (L 29 ± 6%) as seen in Table A5A (Appendix). The latter chiefly consist of very low rank to medium rank and subordinately high rank metapelite-metapsammite grains (Garzanti and Vezzoli, 2003), indicating provenance from a collisional orogen (Dickinson, 1985). Volcanic grains are mainly felsitic and are significant (Lv 8 ± 1%), suggesting subordinate contributions from a volcanic arc. Transparent heavy-mineral assemblages in the Andaman Flysch (Table A5B, Appendix) have very low concentrations (0.3 ± 0.2%). Ultrastable species (zircon, tourmaline, rutile, chromian spinel) represent 21 ± 2% of the assemblage, and ferromagnesian minerals (pyroxenes, amphiboles) are invariably absent, clearly showing the strong influence of diagenetic dissolution.

The very coarse grained sandstones of the Namunagarh Grit Formation chiefly consist of plagioclase and microlitic, lathwork, and felsitic volcanic grains. The quartz content is low (Q 14 ± 10%), and only a few K-feldspar and granitic lithic grains

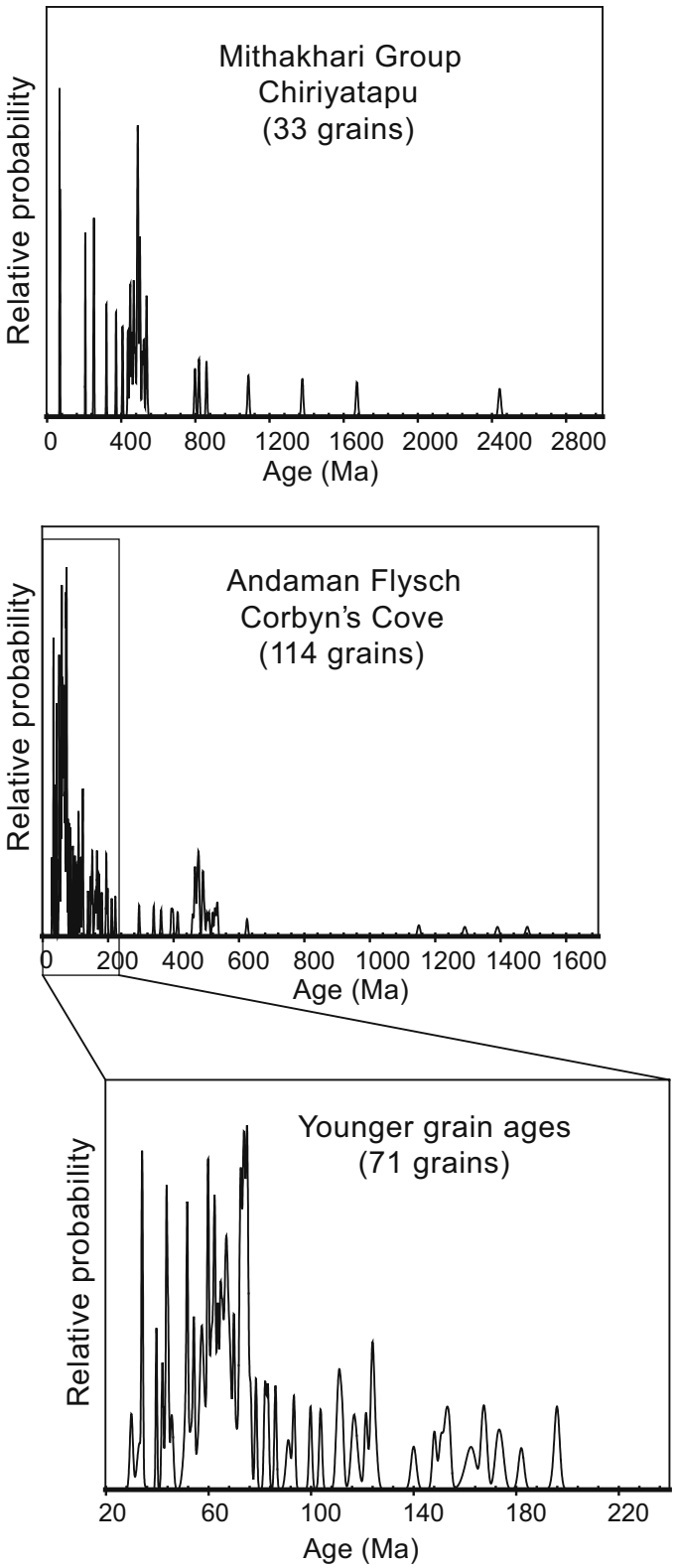

Figure 13. Probability plots showing the distribution of detrital argon mica ages analyzed in this study.

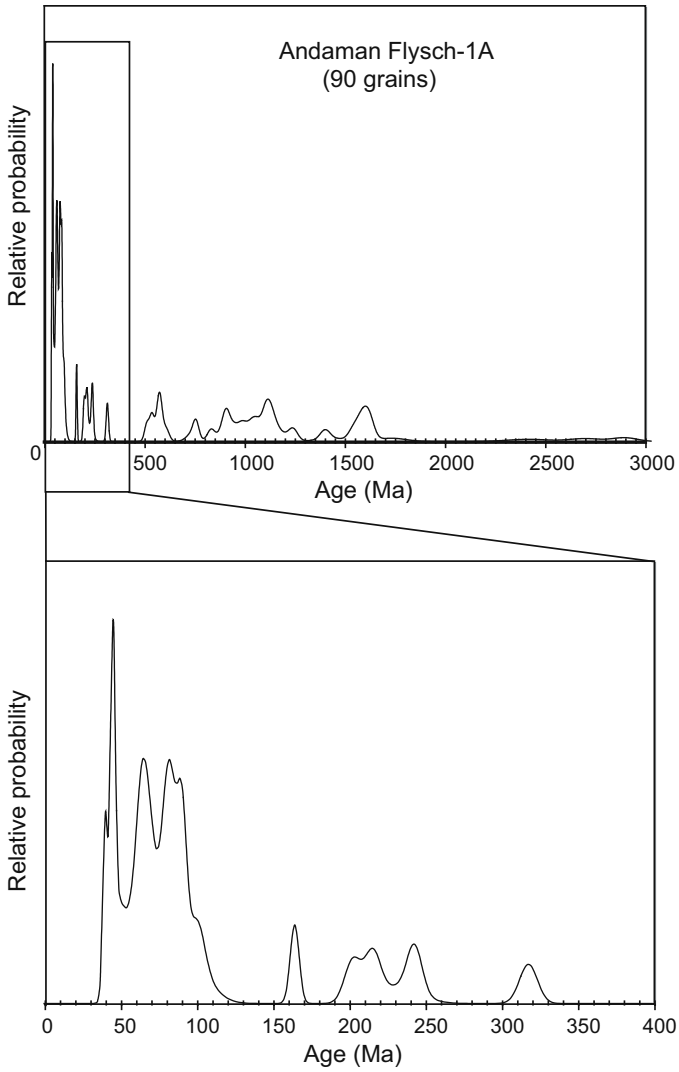

Figure 14. Probability plots showing the distribution of concordant detrital zircon U-Pb ages analyzed in this study.

occur, indicating provenance from a largely undissected volcanic arc (Marsaglia and Ingersoll, 1992). A few terrigenous (shale-sandstone) and very low rank to medium rank metapelite and metapsammite grains also occur, suggesting minor reworking of sedimentary and low-grade metasedimentary sequences. Significant chert, along with traces of metabasite and serpentinite grains, point to minor contributions from oceanic rocks.

In the Namunagarh Grit Formation, opaque grains represent 21 ± 16% of total heavy minerals. Transparent heavy-mineral assemblages have poor concentrations, pointing to significant diagenetic dissolution. These mainly include pyroxenes (mostly green augite; 35 ± 24%) and epidote (34 ± 19%), with subordinate sphene (11 ± 8%), green-brown hornblende (8 ± 8%), chromian spinel (8 ± 8%), minor apatite (2 ± 1%), garnet, rutile, and other

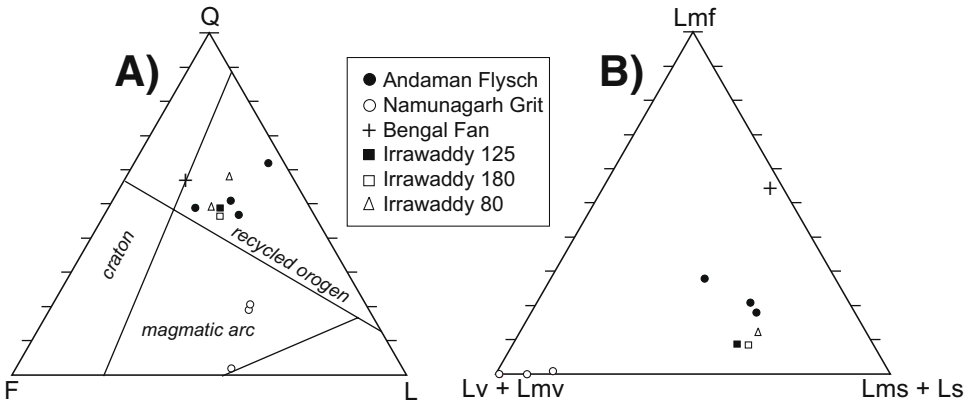

Figure 15. Petrography of Tertiary sandstones of South Andaman. Whereas composition of the Namunagarh Grit Formation sandstones points to provenance from an undissected-transitional magmatic arc, a recycled orogenic provenance is clearly indicated for the Andaman Flysch (Dickinson, 1985). These very fine to fine-grained turbidites compare closely with modern sands of homologous grain size from the Irrawaddy Delta. Q—quartz; F—feldspars; L—lithic grains; Lv + Lmv—volcanic and low-rank metavolcanic; Ls + Lms—sedimentary and low-rank metasedimentary; Lmf—high-rank metamorphic.

titanium oxides, consistent with provenance from a volcanic arc. It must be kept in mind, however, that the original composition of the Namunagarh Grit Formation sandstones (abundant volcanic glass and ferromagnesian minerals) was markedly different with respect to orogen-derived turbidites, and therefore that dissolution reactions of ferromagnesian minerals may have progressed at different rates and in the presence of partially buffered or even saturated interstitial waters.

Sm-Nd Whole Rock and Single Grain Analyses

Sandstone and mudstone samples from the Mithakhari Group yielded whole rock εNd values of –7.2 and 3.1(+), respectively. The Andaman Flysch samples gave whole rock values of εNd –11.1 and –8.2 for the sandstone sample and mudstone sample, respectively. Such values are lower than those of Himalayan sources, which typically range between εNd –12 and –26 (Galy and France-Lanord., 2001) and are inconsistent with Indian Shield sources (Peucat et al., 1989). Very little data exist for the relevant Myanmar source regions. Analyses of modern river sediment from the Irrawaddy River give εNd values between –10.7 (Colin et al., 1999) and –8.3 (this paper: Table 2). The Western Indo-Burman ranges (Fig. 16), which may have been exhuming by the Oligocene (Mitchell, 1993), have more negative values (Colin et al., 2006; Singh and France-Lanord, 2002; this paper, Table 2, and Table A6A, Appendix). Figure 16, which compares the whole rock data from the Andaman Flysch with possible source areas, shows that the most probable source area lies within Myanmar.

To understand the source area in more detail, and in particular the significance of apatite from the Andaman Flysch, which appears to come from more distant sources in comparison with local arc and ophiolite sources in the Mithakhari Group sedimentary rocks, Nd isotope composition was measured on single grains of apatite from the Andaman Flysch. Apatite typically has Sm/Nd ratios of 0.2–0.5, therefore for non-age–corrected apatite the $^{143}Nd/^{144}Nd$ ratio tends to reflect the Nd isotopic composition of their parent whole rock, enabling a direct linkage between thermochronometric data and source in terms of Nd isotopic signature. This approach is particularly effective if the source rocks are young and/or their potential range of Sm-Nd has been quantified. It is also important to note that this approach yields information that is not the same as sediment whole rock values that record an average value (weighted by Nd concentration) of source rocks. It is also possible that the detrital apatite may be dominated by a single apatite-rich source. The majority (~60%) of the single grain analysis of apatite from the Andaman Flysch produced εNd values of –5 to +5, typical of juvenile volcanic whole rock values and contrasting significantly with the bulk sediment values of εNd –11.1 and –8.2 (Fig. 17; Table A6A, B, Appendix). The restricted range of εNd values for these apatites, which gave partially reset FT ages between 30 and 40 Ma (Table A1, Appendix), imply a single source region for the apatite grains. Little is known about the apatite Sm-Nd systematics for the source rocks of the Andaman Flysch. However, as Figure 17 shows, the Andaman Flysch apatite Nd isotope data contrast with apatite Nd data from a Holocene sand dominated by Himalayan sources collected from the Bengal Basin near Joypur, West Bengal. This plot clearly shows that there is little evidence for material eroded from Himalayan sources in this sample.

DISCUSSION

Constraints on Sedimentation and Uplift

New thermochronometric evidence and field observations from type locations on South Andaman, combined with existing biostratigraphy and petrography, provide an improved chronology for deposition and uplift. The accretionary setting means that sedimentation history will be intimately tied to subduction

TABLE 2. TYPICAL SIGNATURES OF POTENTIAL SOURCE REGIONS

Source region	Rock description, heavy minerals, and petrography	Sm–Nd Whole rock εNd(0)	U-Pb ages of zircons	^{40}Ar-^{39}Ar ages of white mica	Zircon fission-track ages
		Himalaya (Southern Flank)			
Drained by Ganges and tributaries *Oligocene bedrock* characteristics interpolated from Eocene and Miocene foreland basin rocks *Bedrock signal today* taken from modern river sediments; higher Himalaya dominates detritus	In the Oligocene, less metamorphosed "Higher Himalayan protolith" would likely have been exposed. Rocks were low-grade metamorphic, sub-garnet grade, nonmicaceous (as determined from Miocene foreland basin rocks).[1]	*Signature today:* Higher Himalayan as determined from Ganges: av. –17.5[2] *Oligocene bedrock:* Eocene: av. –8[3] Miocene: –14 to –17[4]	*Signature today:* As determined from Ganges sediments: mostly >400 Ma–Precambrian. Grains <30 Ma rare. Grains 30–400 Ma very rare[5] *Oligocene bedrock:* Eocene and Miocene: Tertiary grains absent; 65–400 Ma grains very rare[6]	*Signature today:* As determined from Ganges tributaries: Neogene peak; subordinate grains spanning to Precambrian[7] *Oligocene bedrock:* Micas absent in Eocene, very rare in late Oligocene–Miocene[8]	*Signature today:* No FT data available for Ganges sediment; He data <55 Ma, Pliocene–Pleistocene peak[9] *Oliogocene bedrock:* Eocene: peaks at 45 Ma, 119 Ma, and 343 Ma;[10] Miocene: peaks at 30 Ma, 60–75 Ma, 117 Ma, 300–370 Ma[11]
		Burma			
Region drained by Irrawaddy Data from modern Irrawaddy River sediment. Shan-Thai block lies to east, forearc-backarc of Indo-Burman Ranges (IBR) to west. Paleocontinental margin.	Cretaceous arc rocks and Triassic forearc-backarc sediments on metamorphic basement. Mogok schists, gneisses, and intrusives, Shan-Thai Proterozoic–Cretaceous sedimentary rocks on schist basement. Irrawaddy River sediment plots in "recycled orogenic" province field of QFL plot (Dickinson, 1985).[12]	Irrawaddy: –10.7, –8.3[13]	Irrawaddy: Proterozoic, Ordovician, Jurassic–Cretaceous, Paleogene, and Neogene grains[14]	Irrawaddy: Cretaceous to Miocene grains; peak 30–55 Ma[15]	Irrawaddy: Neogene, Paleogene, Cretaceous grains[15]
Western Indo-Burman Ranges Accretionary prism; may have been exhuming and thus a sediment source in late Eocene–Oligocene. Data determined from Arakan modern river sands (R. Allen et al., unpublished data) unless otherwise stated.	Dark-gray, very fine grained volcanic arenite of Eocene (Oligocene?) age. Only limited mica and heavy minerals. Many shale and siltstone lithics.[16]	3 samples give values of –4.0; 1 sample (farther north) gives a value of –7.4[16]	Precambrian: Archean and Proterozoic; Cretaceous and Paleogene (55–65 Ma) grains[16]	No mica present in pre-Miocene sedimentary rocks[16]	Cretaceous and Paleocene to Eocene grains[16]
		Indian Shield			
Dominantly Arc hean craton. Subordinate Proterozoic mobile belts and Gondwanan sedimentary cover.	Predominantly gneisses and granites; opaques, orthoproxene, and sillimanite found in rivers draining east craton.[17]	Values from south and east craton only; –30 to –36[18]	Dominantly Archean[19]	No data available	No data available

[1]Najman and Garzanti (2000).
[2]Galy and France-Lanord (2001).
[3,4]Robinson et al. (2001); Najman et al. (2000).
[5]Campbell et al. (2005).
[6]DeCelles et al. (2004).
[7]Brewer et al. (2003); Najman and Pringle (unpublished data).
[8]DeCelles et al. (1998); Najman and Garzanti (2000).
[9]Campbell et al. (2005).
[10]Najman et al. (2005).
[11]Najman et al. (2004, 2005).
[12]Mitchell (1993); Pivnik et al. (1998); Bertrand et al. (1999); R. Allen et al. (unpublished data).
[13]Colin et al. (1999); R. Allen et al. (unpublished data).
[14]Bodet and Schärer (2000).
[15]R. Allen et al. (unpublished data).
[16]R. Allen et al. (unpublished data).
[17]Mallik (1976).
[18]Peucat et al. (1989); Saha et al. (2004).
[19]Mishra and Rajamani (1999); Auge et al. (2003).

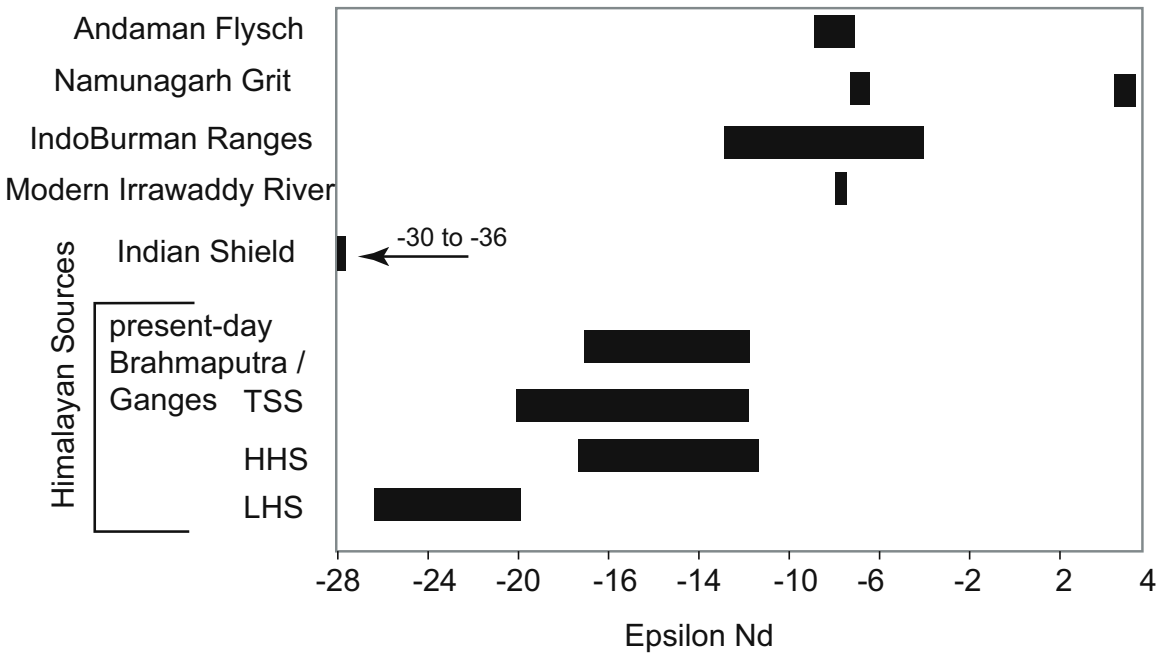

Figure 16. Plot comparing Sm-Nd whole rock values from the Namunagarh Grit Formation and Andaman Flysch Formation with data from possible source regions (Colin et al., 2006; DeCelles et al., 2004; Peucat et al., 1989; Singh and France-Lanord, 2002). The data do not support the Himalayan region as the main source. TSS—Tethys Sedimentary Sequence; HSS—Higher Himalayan Sequence; LHS—Less Himalayan Sequence.

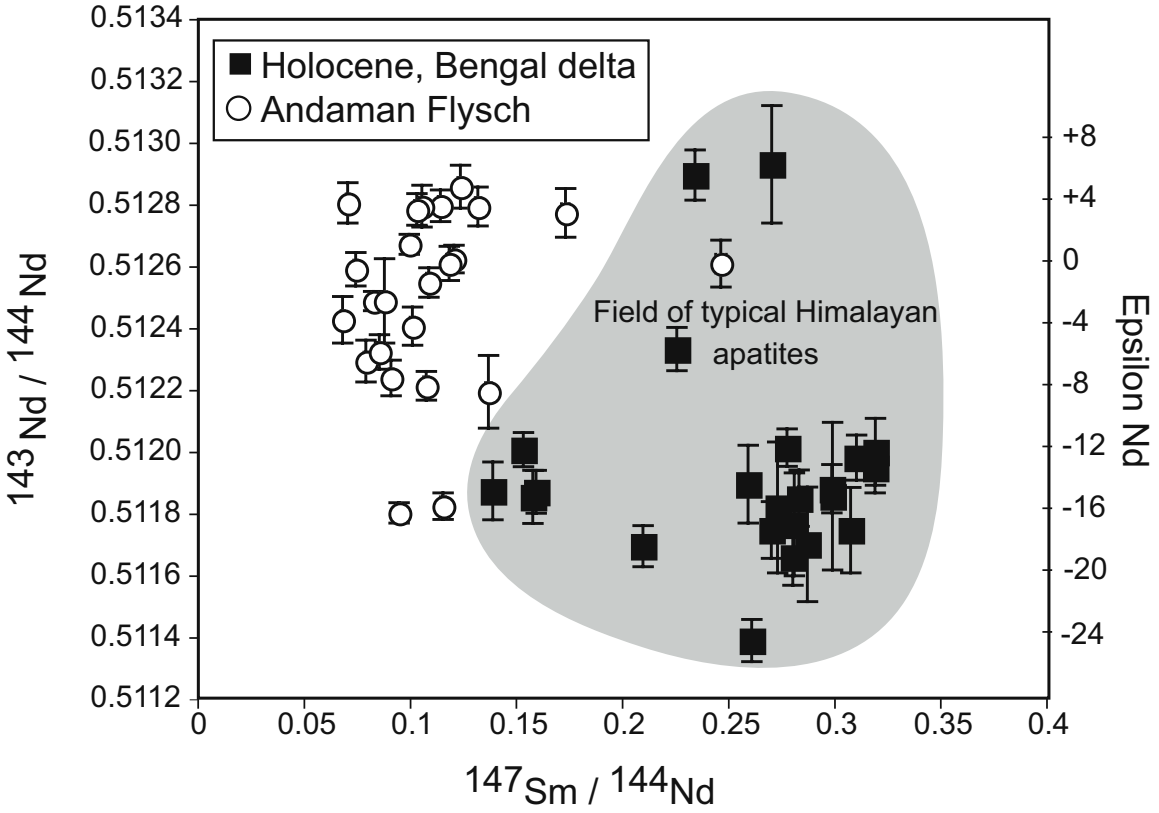

Figure 17. Single grain Nd measured on apatite from the Andaman Flysch Formation compared with a Holocene sand from the Bengal Basin known to have its source in the Himalayas. The clear difference between these two samples supports the Sm-Nd whole rock data plotted in Figure 16.

behavior, offscraping, accretion, and uplift. While in such a setting uplift may be viewed as a more or less continuous process, we recognize some distinct uplift events that have affected the South Andaman geology.

The earliest conglomerates and grits of the Mithakhari Group record subaerial exposure and erosion of the arc sequence and shallow marine limestone cover, as described above, constraining the age of ophiolite as pre–Mithakhari Formation (early to middle Eocene) and post–shallow marine sedimentation. The petrography of the Mithakhari Group is indicative of an undissected volcanic arc with minor reworking of sedimentary and low-grade metasedimentary sequences and minor contributions from oceanic igneous rocks.

Our data provide maximum and minimum age constraints for deposition of the Andaman Flysch. Detrital Ar-Ar mica and FT data constrain maximum depositional age to ca. 30 Ma. The minimum depositional age is constrained by the thermal history modeling, which indicates that burial to maximum temperatures of ~90 ± 5 °C was reached ca. 25–20 Ma, ending with a phase of rapid cooling at ca. 20 Ma. This implies a discrete episode of major uplift at ca. 20 Ma consistent with deposition of the Archipelago Group shallow marine volcanic-rich sedimentary rock from ca. 18 Ma onward (Pal et al., 2005; Singh et al., 2000), which was deposited on top of the Andaman Flysch. Uplift at ca. 20 Ma is also regionally significant, coinciding with major stratigraphic changes in the Irrawaddy Delta, Mergui Basin (Fig. 1), in sediments accreted onto the Andaman-Nicobar Ridge (Curray, 2005), and formation of an unconformity in the Indo-Burman Ranges (Acharyya et al., 1989). Uplift of the Andaman Ridge at 20 Ma is also coincident with the uplift of the Owen and Murray Ridges in the Arabian Sea (Mountain and Prell, 1990), suggestive of a wider plate tectonic trigger.

An outstanding question is, what was the original maximum thickness of the Andaman Flysch? Hydrocarbon-exploration

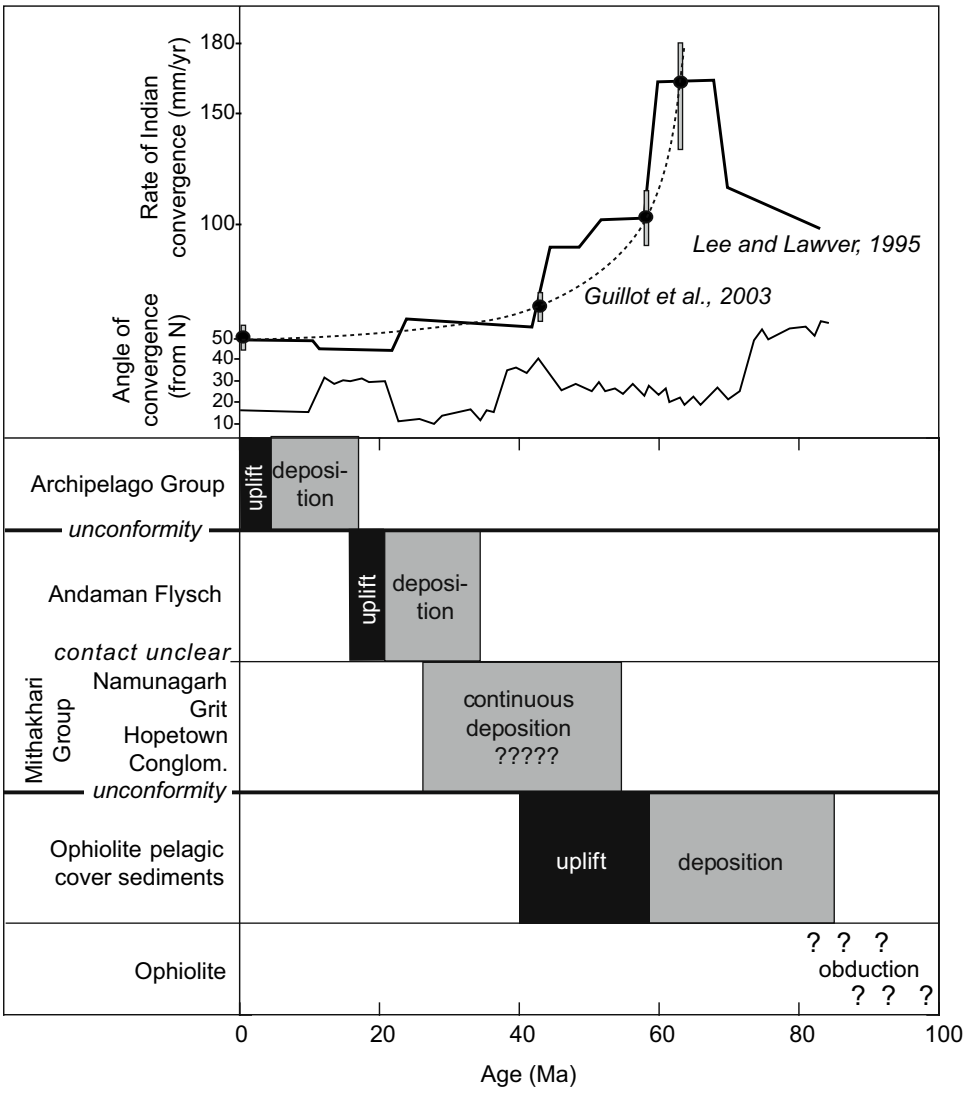

Figure 18. A comparison between Indian convergence history (after Lee and Lawver, 1995, and Guillot et al., 2003) and the uplift and sedimentation history of the rocks studied from South Andaman Island.

wells drilled to the east and the west of Middle Andaman indicate thicknesses of <1000 m (Roy, 1992), whereas outcrop estimates range from ~750 to 3000 m (Pal et al., 2003). Results from thermal history modeling indicate burial of the sampled Andaman Flysch beds beneath at least 2.5 km of cover (assuming geothermal gradients in the range of 35–30 °C). In a growing accretionary wedge, burial is as likely to be due to thrust stacking as it is to sedimentation. Crucially ~2.5 km of burial is incompatible with the unannealed apatite data from the stratigraphically lower Mithakhari Group, highlighting the fact that these different units must have been deposited in different locations (sub-basins?) within the accretionary wedge. Thermal history modeling also shows a phase of accelerated cooling from ca. 10 to 5 Ma. This is probably tied to a phase of regional Miocene–Pliocene uplift linked to spreading in the Andaman Sea driven by increases in the subduction rate and dip of the subducted slab (Khan and Chakraborty, 2005). This last phase of uplift, the result of squeezing between subduction in the west and extension in the east, is likely responsible for the present topography of the Andaman Islands.

The relationship of these episodes of uplift and erosion to regional events can be appreciated when these new constraints are compared against reconstructions of Indian plate convergence history. Figure 18 plots the India-Asia convergence rate and convergence angle from the studies of Lee and Lawver (1995) and more recently from that of Guillot et al. (2003). The graph shows that the studied outcrops of Andaman Flysch were deposited at a time of more northerly convergence and ended when subduction shifted to a less oblique angle. Seismic lines taken from across the Andaman Arc show how the angle of subduction can influence wedge development where the intensity of deformation, which increases from north to south, changes with obliquity of subduction (Curray, 2005). This relationship may explain the evidence for a discrete episode of uplift, involving the Corbyn's Cove Andaman Flysch, at ca. 20 Ma.

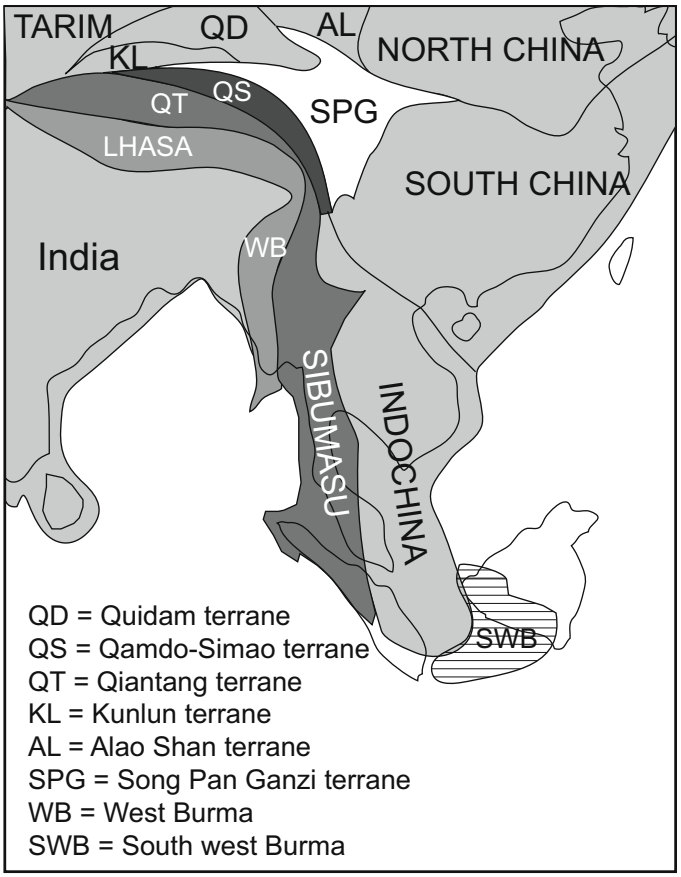

Figure 19. Map showing the principal terranes that have amalgamated to form SE Asia (after Metcalfe, 1996).

Sediment Provenance

The Mithakhari Group shows clear evidence of a dominant contribution from an arc, in keeping with its interpreted forearc basin depositional environment and in line with previous provenance work on the basis of petrography (Bandopadhyay, 2005). The rocks plot in the magmatic arc field on the QFL petrographic plot (Fig. 15); volcanic fragments and glass shards are common, and mineral grains, e.g., apatite, are euhedral. A positive whole rock εNd signal (+3) is indicative of derivation from a mafic-juvenile source. The source was likely that of the Cretaceous–Eocene arc that stretched from the Himalaya collision zone through Myanmar to Sumatra (Mitchell, 1993), as reflected in the FT ages of the euhedral apatites. A subordinate continental source is confirmed by petrography and Precambrian–Paleozoic Ar-Ar mineral grain ages. Such a source was probably the continental margin of the Shan-Thai Block (Sibumasu) extending down to peninsular Thailand, adjacent to the forearc (Metcalfe, 1996) (Fig. 19).

The data show a clear change in petrographic and isotopic characteristics between the Mithakhari Group and the overlying Andaman Flysch. Andaman Flysch composition represents the first sedimentary material to plot in the recycled orogenic province (Fig. 15). Initial results from the pilot study of Sm-Nd whole rock values differ markedly between the Mithakhari Group and the Andaman Flysch, particularly when the finer grained facies are compared. The positive εNd signal of the Mithakhari Group contrasts strongly with the more negative εNd signal (–11) of the Andaman Flysch mudstone, suggestive of a contribution from older continental crustal sources (Fig. 15). Detrital micas are of radically different ages, with the age peaks for the Mithakhari Group falling within the Precambrian–Paleozoic spectrum, whereas those from the Andaman Flysch are typically of late Mesozoic and Tertiary age (Fig. 13). A provenance contrast is not apparent from the zircon FT data (Figs. 9 and 10), as the detrital modes are similar. The apatite FT data cannot be directly compared, as the Andaman Flysch apatites have seen some post-depositional partial resetting. However, comparison of apatite

chemistry (chlorine-uranium content, Fig. 11) does highlight a major difference in the apatite source.

To some extent these differences between the Mithakhari Group and the Andaman Flysch may reflect different mixtures of the same sources. The continental-derived material that dominates the Andaman Flysch represents only a minor contribution in the arc-dominated Mithakhari Group. Variations may have as much to do with depositional setting than source variation. In this regard, sedimentary rocks of the Namunagarh Grit Formation may represent a perched forearc basin, whereas the Andaman Flysch represents deep-water turbidites.

It was proposed by Karunakaran et al. (1968) and Pal et al. (2003) that these "recycled orogenic" Andaman Flysch rocks were sourced by the Irrawaddy River of Myanmar and deposited in a forearc basin. In contrast, Curray et al. (1979) considered the Andaman Flysch to be trench sediments offscraped from the Himalayan-derived Bengal Fan on the downgoing Indian slab. Significant contribution from the northward-drifting cratonic Greater India can be ruled out by the dissimilar petrography, Sm-Nd signature, and mineral cooling ages (Fig. 16; Table 2) as well as by the apatite Nd data (Fig. 17). No apatites were measured with significantly negative εNd values (e.g., −30) diagnostic of Indian Shield sources. The mica argon ages older than 50 Ma, present in both the Mithakhari Group and the Andaman Flysch, are consistent with known sources along the western margin of the Shan-Thai Block (Sibumasu) adjacent to the forearc. The presence in the Andaman Flysch of a small but recognizable population of mica ages between 30 and 40 Ma is not consistent with these Sibumasu sources, as the youngest granites on the Thai peninsula are ca. 50 Ma (Charusiri et al., 1993). Possible sources for the Tertiary mica ages might instead include a region affected by India-Asia collision at ca. 50 Ma, possible candidates being either the nascent Himalaya to the north, Transhimalaya, or a more northeastern source—namely, Myanmar locations of the Burman-Thai Block—where Tertiary metamorphism, magmatism, and grain isotopic characteristics and ages are ascribed to the effects of the India-Asia collision (Bertrand et al., 1999; 2001, Bodet and Schärer, 2000; Barley et al., 2003). Isotopic characteristics of these Myanmar rocks are incompletely documented at present. Those that are available are taken from bedrock, and analyses of sands from the Irrawaddy River, which drains the areas under discussion—i.e., the Central Myanmar Basin, to its east the Mogok Belt and Shan Plateau, and to its west the Indo-Burman Ranges (Bodet and Schärer, 2000; Colin et al., 2006; Singh and France-Lanord, 2002; Table 2, this study)—as verified by 30 Ma Ar-Ar ages from the

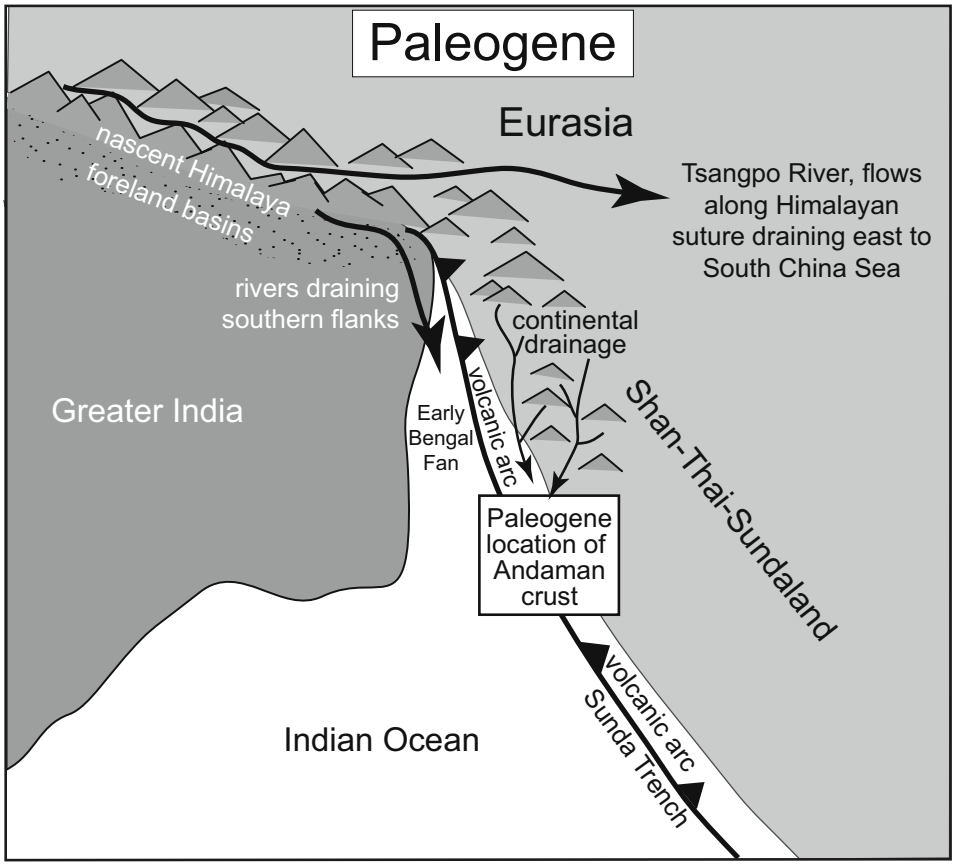

Figure 20. Cartoon illustrating the Paleogene paleogeography and paleodrainage of SE Asia. Although this sketch simplifies the location of the subduction zone, the Asian margin and Andaman crust would have changed throughout the Paleogene as Greater India moved northward. The cartoon does serve to illustrate the general location of continental sources and drainages to the Andaman region.

Irrawaddy region (Table 2). Discrimination between these two possible sources, the Himalayan or Myanmar region, requires an understanding of the different paleogeography and paleodrainage of the region in the Oligocene in comparison with the present day, as discussed below (Fig. 20).

Prior to the India-Asia collision, the northward extension of the Sunda Arc as far as Pakistan permits correlation between the southern margin of Asia in the Himalayan region with equivalent rocks in Myanmar (Mitchell, 1993) and farther south. Subsequent to continental collision at ca. 50 Ma (Rowley, 1996), the Himalayan thrust belt started to develop in the north while the eastern (Myanmar) region remained an active continental margin with, for example, the Central Basin along which the Irrawaddy now drains, the site of the continental margin between the subduction zone to the west and the arc to the east (Pivnik et al., 1998). Movement along the Sagaing dextral strike-slip fault (initiation in pre-Miocene times: Mitchell, 1993) and the opening of the Andaman Sea in the late Miocene (Curray, 2005; Khan and Chakraborty, 2005) were responsible for changes in the coastal paleogeography of this region.

In the Paleogene the Yarlung-Tsangpo River (draining the Himalayan Arc and suture zone) probably drained into the South China Sea prior to its capture by the Irrawaddy River, and finally the Brahmaputra River in the Neogene (Clark et al., 2004, 2005). Thus, Ganges-type rivers—those draining only the southern slopes of the Himalayan mountain belt, with no arc component—would have contributed the Himalayan signal to the Indian Ocean (Fig. 17). The southern slopes of the Himalayas consist of Indian crust. Characteristics of these rocks changed with time as Neogene Himalayan metamorphism subsequently increased the metamorphic grade and overprinted the metamorphic cooling ages of minerals and rocks exposed at the surface today. In contrast, the northeastern Myanmar region was devoid of Indian crustal rocks, and no thrust belt was present to bar the Asian and arc sources from draining south. Prior to the opening of the Andaman Sea, rivers draining the Myanmar region presumably would have drained into the trench-forearc system, which acted as a "sink," preventing deposition farther west onto the Indian plate.

The Andaman Flysch records mixed orogenic and arc provenance. The young (<100 Ma) U-Pb–dated detrital zircons from the Andaman Flysch are consistent with derivation from igneous sources, most likely an eastern (Myanmar) provenance based on similar aged grains found in modern Irrawaddy River sediment (Bodet and Schärer, 2000), as grains with young U-Pb zircon ages are extremely rare in the southern flanks of the Himalayas (Campbell et al., 2005; DeCelles et al., 1998, 2004).

Myanmar sources also can adequately account for the majority of the "recycled orogenic" component of the detritus in the Andaman Flysch. Both petrography and εNd whole rock signatures, especially of the fine-grained material, are nearly identical to those of the modern Irrawaddy River (Figs. 15 and 16). ^{40}Ar-^{39}Ar and FT data from the Irrawaddy River also are similar to data obtained from the Andaman Flysch, showing a mica age peak of ca. 30–60 Ma with a population of older Cretaceous grains and zircon FT ages of Miocene and Paleogene (20–65 Ma) to Cretaceous (Table 2). Nevertheless, some disparities are evident. The lack of zircon grains with Jurassic U-Pb ages for the Andaman Flysch is surprising, considering their prevalence in the Mogok Belt (Barley et al., 2003) and their presence in modern Irrawaddy River sand (Bodet and Schärer, 2000). Recourse to a Himalayan contribution through the Bengal Fan is not required to explain the recycled orogenic component of the Andaman Flysch. However, a minor contribution from the Himalayan thrust belt cannot be ruled out: for example, grains aged 100–1500 Ma in the Andaman Flysch are common to both Himalayan and Myanmar rock types. In addition, the intermediate whole rock εNd values may represent a mixture between a more negative Himalayan source and more positive Myanmar sources, as implied by the single grain apatite analyses. The possibility of dual provenance, with Himalayan-derived Bengal Fan material and Myanmar-derived material meeting and mixing in the trench, is a model that would be consistent with the regional seismic data, which show folding and uplift of Bengal Fan sediments at the base of the slope (Curray, 2005). Definitive discrimination between Myanmar and Himalayan sources, if possible at all, awaits more information on the source rock geology of Myanmar, in particular that of the Shan Plateau and Mogok Belt, and analysis of as-yet-undrilled Oligocene sediments preserved in the Bengal Fan, and coeval sedimentary rocks of the Central Myanmar Basin.

CONCLUSIONS

The Mithakhari Group was deposited in the late Paleocene–Eocene, with a maximum age of ca. 60 Ma. This current study shows that the sedimentary rocks are predominantly arc derived from a proximal source in keeping with the interpreted forearc depositional environment. A subordinate contribution from an older continental source was most likely to have been the western Sibumasu margin, but a Transhimalayan arc unit source cannot be ruled out.

The Oligocene Andaman Flysch was deposited between 30 and 20 Ma, and then uplifted by 20 Ma. It shows a clear change in petrographic and isotopic characteristics from the Mithakhari Group and is composed mainly of "recycled orogenic" sources with a subordinate arc provenance. It represents the earliest record in the region of major influx from a continental area. The recycled orogenic component is most simply explained by erosion from the northeastern (Myanmar) continental region. Isotopic and petrographic differences between formations may be explained to some extent by different mixtures and contributions from the same source regions. Although dual provenance is a favorable model for this region, detailed discrimination between Himalayan and Myanmar sources, at present, awaits more data from Myanmar source rocks.

TABLE A1. FISSION-TRACK ANALYTICAL DATA FOR ANDAMAN ISLANDS–SOUTH ANDAMAN

Sample	Latitude Longitude	Mineral	No. of grains	ρd Nd	ρs NS	ρι Ni	Dispersion ($P\chi^2$)	Dispersion RE%	Central age ±1σ (Ma)	Age components			Mean track length (μm)	S.D.	No. of tracks
MITHAKHARI GROUP															
Hopetown Conglomerate Formation															
Hopetown Quarry	N11°41.407′ E92°43.501′	*Zircon*	*25*	*0.528 (3450)*	*12.16 (4942)*	*4.32 (1756)*	*0.0*	*56.2*	91.8 ± 10.8	***61 ± 2 (16)***	***129 ± 10 (5)***	***280 ± 32 (4)***			
		Apatite	19	1.106 (6131)	0.064 (58)	0.209 (191)	0.03	69.1	56.5 ± 8.5	**57 ± 9 (19)**					
Namunagarh Grit Formation															
Mungleton Quarry	N11°34.223′ E92°39.541′	*Zircon*	*18*	*0.535 (3450)*	*10.972 (4182)*	*4.872 (1857)*	*0.0*	*42.3*	75.15 ± 7.9	***59 ± 2 (15)***		***226 ± 21(3)***			
		Apatite	21	1.106 (6131)	0.150 (322)	0.246 (946)	0.0	64.5	68.9	**55 ± 8 (19)**	**151 ± 68 (1)**	**314 ± 51 (1)**			
Namunagarh Quarry	N11°41.339′ E92°41.106′	Apatite	24	1.106 (6131)	0.060 (108)	0.282 (506)	99.6	0.0	39.8 ± 4.2	**40 ± 4 (24)**					
Chiriyatapu	N11°42.005′ E93°32.301′	*Zircon*	*38*	*0.525 (3450)*	*12.53 (7468)*	*2.255 (1344)*	0.0	92.6	143.0 ± 22	**40 ± 3 (9)**	**91 ± 7 (8)**	**329 ± 17 (22)**			
ANDAMAN FLYSCH															
AND-1A	N11°38.430′ E92°45.292′	Apatite	38	1.106 (6131)	0.264 (497)	1.653 (3116)	0.02	28.8	30.85 ± 2.2	**31 ± 2 (38)**			13.25 ± 0.17	1.51	76
		Zircon	*43*	*0.516 (3450)*	*8.341 (6439)*	*4.07 (3147)*	*0.0*	*44.5*	62.15 ± 4.6	***44 ± 2 (24)***	***67 ± 4 (12)***	***147 ± 10 (6)***			
AND-1B	N11°38.457′ E92°45.318′	Apatite	57	1.106 (6131)	0.499 (738)	2.499 (3696)	7.3	16.3	37.15 ± 1.8	**37 ± 2 (57)**			13.06 ± 0.20	1.75	75
		Zircon	*32*	*0.515 (3450)*	*6.115 (3085)*	*3.685 (1859)*	*0.0*	*41.5*	53.75 ± 4.4	***41 ± 2 (26)***	***101 ± 14 (6)***				
AND-3	N11°38.459′ E92°45.368′	Apatite	50	1.106 (6131)	0.497 (852)	2.556 (4739)	0.03	22.6	35.85 ± 1.9	**36 ± 2 (50)**			13.24 ± 0.22	1.61	54
		Zircon	*15*	*0.108 (3450)*	*10.24 (1930)*	*4.828 (910)*	*0.0*	*73.0*	58.55 ± 11.3	***36 ± 2 (12)***		***616 ± 102 (3)***			
AND-4	N11°39.461′ E92°45.417′	Apatite	47	11.106 (6131)	0.427 (923)	2.652 (5733)	0.04	20.2	30.75 ± 1.5	**31 ± 2 (47)**			13.42 ± 0.23	1.80	62
		Zircon	*42*	*0.505 (3450)*	*10.63 (7575)*	*4.506 (3210)*	*0.0*	*70.1*	67.95 ± 7.6	***38 ± 1 (20)***	***58 ± 4 (10)***	***270 ± 16 (12)***			

Note: (i) Track densities are (x10^6 tr cm^{-2}); numbers of tracks counted (N) shown in brackets. (ii) Analyses by external detector method using 0.5 for the $4\pi/2\pi$ geometric correction factor. (iii) Ages calculated using dosimeter glass CN-5; (apatite) ξ_{CN5} = 338 ± 4; CN-2 (zircon) ξ_{CN2} = 127 ± 4 calibrated by multiple analyses of IUGS apatite and zircon age standards (see Hurford, 1990). (iv) $P\chi^2$ is probability for obtaining χ^2 value for v degrees of freedom, where v = no. crystals –1. (v) Central age is a modal age, weighted for different precisions of individual crystals (see Galbraith and Green, 1990). (vi) Age modes deconvolved using approach of Sambridge and Compston (1994) and Galbraith and Laslett (1993). RE—% relative error about the central age; S.D.—standard deviation; bold type—apatite; bold italic type—zircon ages.

TABLE A2. RAW APATITE-HELIUM DATA

Sample	Location	^{4}He (ncc)	HB (ncc)	^{4}He-HB (ncc)	%S.D. in Q ±	^{4}He (atoms)	Absolute ±	^{238}U (ng)	± (%)	^{232}Th (ng)	± (%)	**He age* (Ma)**	Error ± 7%	Grain radius	FT corrected	FT corrected age (Ma)
AND-A	N11°38.430′ E92°45.292′	0.356	0.023	0.333	0.452	8.95E + 09	4.04E + 07	0.108	1.2	0.537	1.33	**11.704**	0.819	77	0.81	14.4
AND-B	N11°38.457′ E92°45.318′	0.209	0.021	0.188	0.119	5.05E + 09	6.01E + 06	0.062	2.18	0.215	1.8	**13.756**	0.962	66	0.76	18.1
AND-C	N11°38.459′ E92°45.368′	0.222	0.018	0.204	0.119	5.48E + 09	6.52E + 06	0.058	1.98	0.315	1.4	**12.664**	0.886	82	0.81	15.6

Note: All samples are taken from the Andaman Flysch Formation at Corbyn's Cove. Helium ages are based on replicate analyses of apatite grains. The total uncertainty in sample age is based on the reproducibility of 39 analyses at the California Institute of Technology laboratory. Durango apatite standard (this error of the mean = 6.7%) combined with the U/Th and He analytical uncertainties. HB—hot blank; ncc—nanno cc; S.D.—standard deviation; FT—fission track.

*Uncorrected He age.

TABLE A3. RAW ARGON DATA

Andaman Flysch (Corbyn's Cove section)

A1B	^{40}Ar	^{39}Ar	^{38}Ar	^{37}Ar	^{36}Ar	$^{40}Ar^*/^{39}Ar$	±	Age (Ma)	±
Ms 1	0.68068	0.213559	0.003536	0.005284	0.000779	2.109962	0.020067	51.8	0.5
Ms 2	0.203759	0.060257	0.000705	0.000626	6.48E-05	3.063559	0.006231	74.7	0.4
Ms 3	0.451179	0.185698	0.002571	0.002597	0.000354	1.865821	0.022963	45.9	0.6
Ms 4	0.329659	0.110714	0.001661	0.002407	0.000334	2.085147	0.038311	51.2	1.0
Ms 5	0.37799	0.046614	0.000787	0.000994	0.00013	7.286482	0.032957	172.9	1.1
Ms 6	0.269821	0.037161	0.000531	0.000573	5.98E-05	6.784923	0.089994	161.5	2.2
Ms 8	2.277688	0.11746	0.001906	0.002831	0.000274	18.7013	0.031643	414.2	2.0
Ms 9	2.143176	0.070945	0.00093	0.000402	2.99E-05	30.08465	0.047492	626.5	2.8
Ms 10	1.384602	0.074126	0.001043	0.001053	0.00018	17.96253	0.023198	399.5	1.9
Ms 11	0.253605	0.015673	0.000291	5.75E-05	0	16.18154	0.035317	363.6	1.8
Ms 12	0.259847	0.082319	0.00117	0.000824	7.98E-05	2.870187	0.003993	70.1	0.4
Ms 13	3.391288	0.385463	0.004783	0.003164	0.000389	8.499624	0.011701	200.1	1.0
Ms 15	0.790418	0.252174	0.003255	0.003477	0.000284	2.801527	0.02637	68.4	0.7
Ms 16	0.531821	0.070046	0.000772	0.000291	5.49E-05	7.360776	0.036057	174.5	1.2
Ms 17	0.323132	0.105295	0.001329	0.001905	0.000189	2.537016	0.031682	62.1	0.8
Ms 18	0.832588	0.098415	0.001318	0.000894	4.98E-05	8.310543	0.035372	195.9	1.2
Ms 19	0.176399	0.061786	0.00071	0.000428	7.99E-05	2.472932	0.067916	60.5	1.7
Ms 20	0.458665	0.086807	0.001068	0.00179	0.00013	4.842794	0.034779	116.7	1.0
Ms 21	0.269899	0.070387	0.000792	0.000117	0.0002	2.994993	0.047513	73.1	1.2
Ms 22	1.721992	0.356929	0.004472	0.009619	0.000637	4.296717	0.010036	103.9	0.6
Ms 23	1.216759	0.459022	0.005575	0.00187	0.00031	2.451514	0.006712	60.0	0.3
Ms 24	0.085958	0.027352	0.000404	0.000195	0	3.142686	0.011197	76.6	0.5
Ms 25	0.130443	0.038038	0.000618	0.002262	0.000284	1.219882	0.023433	30.1	0.6
Ms 26	2.371162	0.106391	0.001354	0.001404	0.000115	21.96896	0.014042	477.7	2.1
Ms 27	0.314057	0.064276	0.000828	0.000507	4.99E-05	4.656836	0.012754	112.4	0.6
Ms 28	0.336883	0.064142	0.000767	0.000156	8E-05	4.883813	0.04699	117.7	1.2
Ms 29	0.999109	0.106174	0.001329	0.00041	0.000125	9.062499	0.029797	212.6	1.2
Ms 30	0.124323	0.075656	0.000961	0.000488	7.49E-05	1.350842	0.039184	33.3	1.0
Ms 31	1.604755	0.163177	0.001993	0.000528	0.000145	9.572115	0.020485	223.8	1.1
Ms 32	0.176028	0.107915	0.001318	0.000411	8.49E-05	1.398714	0.006655	34.5	0.2
Ms 33	0.094113	0.056227	0.000787	0.000782	5.48E-05	1.385834	0.005724	34.2	0.2

A3	^{40}Ar	^{39}Ar	^{38}Ar	^{37}Ar	^{36}Ar	$^{40}Ar^*/^{39}Ar$	±	Age (Ma)	±
Ms 1	0.274897	0.083084	0.000981	0.00039	0.000145	2.793324	0.037215	68.2	1.0
Ms 2	0.444523	0.143237	0.00185	0.001424	0.000445	2.186142	0.029916	53.6	0.8
Ms 3	0.297818	0.112368	0.0014	0.000746	0.000115	2.348489	0.038715	57.5	1.0
Ms 4	1.30819	0.466538	0.005703	0.002087	0.000109	2.734713	0.013397	66.8	0.5
Ms 5	0.346651	0.128071	0.001671	0.000476	0.000155	2.349362	0.023267	57.6	0.6
Ms 6	3.632999	0.500069	0.006087	0.001156	0.000305	7.084947	0.012826	168.3	0.9
Ms 8	0.311219	0.100244	0.001252	0.000476	0.000185	2.55964	0.004776	62.6	0.3
Ms 9	0.281996	0.054435	0.00068	0.000511	0.000105	4.611138	0.010622	111.3	0.6
Ms 10	0.180333	0.044863	0.000593	0.000392	2.49E-05	3.855628	0.00766	93.5	0.5
Ms 11	0.518299	0.095269	0.001186	0.000528	0.000125	5.053064	0.006582	121.6	0.6
Ms 12	0.604087	0.186293	0.002397	0.000648	0.000155	2.997079	0.016331	73.1	0.5
Ms 13	0.514859	0.086648	0.001109	0.000392	2.49E-05	5.857044	0.034464	140.2	1.0
Ms 15	0.190225	0.061068	0.000797	0.000672	0.000145	2.414197	0.048452	59.1	1.2
Ms 16	0.138431	0.029423	0.000409	0.000534	0.000115	3.551304	0.003826	86.3	0.4
Ms 17	0.560451	0.085584	0.001022	6.89E-05	6.5E-05	6.324168	0.019494	151.0	0.9
Ms 18	1.927513	0.246058	0.003455	0.002792	0.000814	6.855692	0.06817	163.1	1.7
Ms 19	0.549605	0.188385	0.002402	0.00138	0.000265	2.502356	0.018307	61.2	0.5
Ms 20	0.199519	0.062808	0.000767	0.000897	0.000185	2.307352	0.05385	56.5	1.3
Ms 21	0.792813	0.159513	0.00209	0.002278	0.000214	4.573025	0.019797	110.4	0.7
Ms 22	0.531614	0.155877	0.00209	0.001657	0.000385	2.681443	0.009091	65.6	0.4
Ms 23	0.290937	0.092139	0.001272	0.000881	7.98E-05	2.901768	0.033228	70.8	0.9
Ms 24	0.481724	0.087635	0.000905	0.00038	9.99E-05	5.160096	0.036978	124.1	1.0
Ms 25	1.163152	0.352631	0.004461	0.001418	0.00038	2.980373	0.009667	72.7	0.4
Ms 26	0.272653	0.094083	0.001191	0.005552	8.85E-05	2.619921	0.032203	64.1	0.8
Ms 27	0.422343	0.128727	0.00161	0.000571	0.00011	3.028746	0.023467	73.9	0.7
Ms 28	0.24212	0.086183	0.001145	0.000242	9.94E-06	2.775297	0.03496	67.8	0.9
Ms 29	0.358268	0.11507	0.001441	0.000277	2.99E-05	3.036643	0.005754	74.1	0.4
Ms 30	0.178945	0.044807	0.000537	0.000211	3.49E-05	3.763259	0.033264	91.3	0.9
Ms 31	0.273151	0.093756	0.001232	0.000316	0.000115	2.551233	0.016583	62.4	0.5
Ms 32	0.173772	0.089489	0.00115	1.76E-05	5E-05	1.77673	0.016944	43.7	0.5

(*continued*)

TABLE A3. RAW ARGON DATA (*continued*)

Andaman Flysch (Corbyn's Cove section)

A4	^{40}Ar	^{39}Ar	^{38}Ar	^{37}Ar	^{36}Ar	$^{40}Ar^*/^{39}Ar$	±	Age (Ma)	±
Ms 1	1.757257	0.228175	0.003051	0.001952	0.000479	7.080388	0.0316	168.2	1.1
Ms 2	0.350481	0.117885	0.001625	0.000598	0.000135	2.63508	0.030076	64.4	0.8
Ms 3	0.226229	0.086674	0.001165	0.000669	0.000115	2.218651	0.038875	54.4	1.0
Ms 4	0.84056	0.203536	0.00254	0.000722	0.000305	3.687254	0.018742	89.5	0.6
Ms 5	0.387886	0.07517	0.001007	0.000476	3.49E-05	5.023023	0.044232	120.9	1.2
Ms 6	0.827359	0.256024	0.00326	0.001164	0.00039	2.781793	0.00436	68.0	0.3
Ms 8	0.124755	0.077014	0.001012	0.000247	0.00011	1.198084	0.007833	29.6	0.2
Ms 9	3.009747	0.428003	0.005417	0.000953	0.000195	6.897607	0.010471	164.0	0.8
Ms 10	1.209192	0.187151	0.00232	0.000706	0.000105	6.29557	0.006128	150.3	0.7
Ms 11	0.497906	0.161033	0.00184	0.000212	7.49E-05	2.954419	0.018552	72.1	0.6
Ms 12	3.00958	0.046496	0.000608	0.000395	7.99E-05	64.22046	0.067476	1144.9	4.3
Ms 13	0.239454	0.097718	0.001129	0.000897	0.00013	2.058057	0.005784	50.5	0.3
Ms 15	1.727941	0.097393	0.001247	3.59E-05	7.5E-05	17.51444	0.014541	390.6	1.8
Ms 16	0.259758	0.122808	0.001441	0.000395	3.49E-05	2.0312	0.024229	49.9	0.6
Ms 17	0.102435	0.029899	0.000307	0	1.5E-05	3.277664	0.007241	79.8	0.4
Ms 18	0.565702	0.067938	0.000869	0.000198	3.49E-05	8.174691	0.007531	192.8	0.9
Ms 19	0.461503	0.030601	0.000363	0	5E-06	15.03286	0.049761	340.1	1.9
Ms 20	0.084844	0.03198	0.000358	3.6E-05	9.99E-06	2.560674	0.046289	62.7	1.2
Ms 21	0.051231	0.028354	0.000327	0.000144	9.96E-06	1.70302	0.116858	41.9	2.9
Ms 22	0.539888	0.175027	0.002034	0.000648	0.000225	2.705021	0.007126	66.1	0.4
Ms 23	0.224278	0.125809	0.001584	0.000793	0.000115	1.513072	0.003637	37.3	0.2
Ms 24	2.435008	0.11556	0.001303	0.000343	8.99E-05	20.84143	0.030878	456.1	2.1
Ms 25	0.28137	0.043934	0.000537	0.000162	3E-05	6.202931	0.034616	148.2	1.1
Ms 26	1.447467	0.066026	0.00092	0.001368	0.000185	21.09624	0.0327	461.0	2.1
Ms 27	0.131921	0.043514	0.000777	0.001825	0.000255	1.303279	0.01007	32.2	0.3
Ms 28	0.381247	0.061408	0.000899	0.001902	0.000264	4.935659	0.026829	118.9	0.8
Ms 29	0.400761	0.030962	0.000603	0.001484	0.000155	11.46811	0.056235	265.1	1.7
Ms 30	0.124287	0.055912	0.000761	0.001294	0.000205	1.141272	0.059711	28.2	1.5
Ms 31	0.077119	0.024908	0.000368	0.000686	8.98E-05	2.030571	0.013455	49.9	0.4
Ms 32	0.042558	0.024805	0.000409	0.000952	4.97E-05	1.123077	0.119683	27.7	2.9
Ms 33	0.057102	0.020714	0.000225	0.000305	5.99E-05	1.901885	0.160137	46.7	3.9

Mithakhari Group, Chiriyatapu

	^{40}Ar	^{39}Ar	^{38}Ar	^{37}Ar	^{36}Ar	$^{40}Ar^*/^{39}Ar$	±	Age (Ma)	±
Ms 1	0.8284261	0.0365259	0.0004242	0.0004699	0.0000000	22.6805064	0.0750144	491.3	2.6
Ms 2	0.7446774	0.0323472	0.0003628	0.0000000	0.0000550	22.5188268	0.0957791	488.2	2.8
Ms 3	0.7987535	0.0472551	0.0006388	0.0002743	0.0000249	16.7471471	0.0197808	375.1	1.7
Ms 4	0.3026851	0.0938337	0.0011243	0.0001764	0.0000750	2.9897197	0.0315933	72.9	0.8
Ms 5	0.6288437	0.0690488	0.0008483	0.0003334	0.0000449	8.9150267	0.0157014	209.3	1.0
Ms 6	0.2056404	0.0084045	0.0001022	0.0000000	0.0000000	24.4679238	0.0604556	524.8	2.5
Ms 8	2.0267770	0.0181880	0.0002760	0.0003637	0.0000349	110.8679577	0.1272294	1674.6	5.6
Ms 9	1.3058958	0.0589862	0.0007666	0.0002830	0.0000949	21.6634575	0.0479489	471.9	2.3
Ms 10	1.0895856	0.0467023	0.0006133	0.0004044	0.0000849	22.7933251	0.0380826	493.4	2.3
Ms 11	1.7582128	0.0745294	0.0008279	0.0005462	0.0000899	23.2345815	0.0322423	501.7	2.3
Ms 12	0.7200124	0.0307043	0.0004191	0.0003844	0.0001499	22.0072636	0.1088272	478.5	3.0
Ms 13	0.7633280	0.0327602	0.0004344	0.0003442	0.0000499	22.8502553	0.0157553	494.5	2.2
Ms 15	1.4321915	0.0604223	0.0007308	0.0002229	0.0000499	23.4587880	0.0323211	506.0	2.3
Ms 16	3.1189393	0.0694722	0.0008943	0.0007095	0.0000998	44.4702431	0.0356104	863.3	3.5
Ms 17	0.5782068	0.0518422	0.0006746	0.0002434	0.0000349	10.9540815	0.0577358	254.0	1.7
Ms 18	1.2848422	0.0599626	0.0007052	0.0001623	0.0000750	21.0580001	0.0540885	460.2	2.3
Ms 19	0.5290525	0.0217523	0.0003015	0.0002639	0.0000199	24.0509065	0.1038536	517.1	3.0
Ms 20	5.1561196	0.0246141	0.0003628	0.0002639	0.0000799	208.5188362	0.2883512	2444.9	6.9
Ms 21	0.6433217	0.0339743	0.0003577	0.0001625	0.0000500	18.5010347	0.0472177	410.2	2.1
Ms 22	1.1030049	0.0956311	0.0011039	0.0005283	0.0001499	11.0708902	0.0175933	256.5	1.3
Ms 23	0.3852341	0.0186428	0.0002044	0.0000000	0.0000000	20.6639642	0.0133670	452.6	2.0
Ms 24	0.8201835	0.0345528	0.0004804	0.0002349	0.0000499	23.3100383	0.0867000	503.2	2.7
Ms 25	0.2651809	0.0818851	0.0009965	0.0008358	0.0001048	2.8603315	0.0027919	69.8	0.3
Ms 26	0.4454907	0.0287515	0.0004242	0.0007315	0.0001248	14.2118131	0.0282976	323.1	1.6
Ms 27	0.2823107	0.0124546	0.0001073	0.0000000	0.0000000	22.6671453	0.0457513	491.0	2.3
Ms 28	7.5439887	0.1794691	0.0021310	0.0008891	0.0001048	41.8625264	0.0295576	822.6	3.3
Ms 29	0.4338841	0.0171655	0.0002402	0.0000000	0.0000000	25.2765779	0.0434406	539.8	2.5
Ms 30	0.9228281	0.0225529	0.0003373	0.0004192	0.0000299	40.5267640	0.1467725	801.4	4.0
Ms 31	2.4734857	0.0295677	0.0004191	0.0005765	0.0000398	83.2566784	0.1423053	1380.1	5.1
Ms 32	1.5381052	0.0256109	0.0003475	0.0004719	0.0000000	60.0566236	0.1661772	1089.0	4.7
Ms 33	0.3426377	0.0155174	0.0001942	0.0002623	0.0000299	21.5108920	0.0746433	469.0	2.5

TABLE A4. ZIRCON U-Pb DATA (UNCORRECTED AGES) FOR ANDAMAN FLYSCH SAMPLE 1A

Grain no.	$^{206}Pb/^{238}U$ ratio	±	$^{207}Pb/^{235}U$ ratio	±	$^{207}Pb/^{206}Pb$ ratio	±	$^{206}Pb/^{238}U$ Age (Ma)	±1σ	$^{207}Pb/^{235}U$ Age (Ma)	±1σ	$^{207}Pb/^{206}Pb$ Age (Ma)	±1σ
8	0.56820	0.01491	18.27837	0.00211	0.23368	0.01172	2900.4	61.3	3004.5	46.4	3077.4	77.9
21	0.52114	0.01876	17.80391	0.00319	0.24751	0.01869	2704.0	79.5	2979.2	72.0	3168.9	114.9
18	0.45548	0.02377	10.17671	0.00390	0.16214	0.01534	2419.6	105.3	2451.0	83.7	2478.1	151.3
28	0.30919	0.01417	5.34072	0.00228	0.12476	0.01304	1736.7	69.8	1875.4	88.2	2025.4	174.4
1	0.25134	0.01476	3.17496	0.00192	0.09164	0.01199	1445.4	76.0	1451.1	95.3	1459.9	230.3
37	2.68537	0.14191	0.23801	0.00394	0.08188	0.00394	1376.4	20.5	1324.4	39.1	1242.7	99.7
7	0.20471	0.00761	2.27006	0.00089	0.08055	0.00685	1200.5	40.7	1203.0	56.6	1210.5	158.8
13	0.19499	0.00490	2.12506	0.00101	0.07915	0.00497	1148.4	26.5	1157.0	42.0	1175.9	119.3
31	2.04475	0.18301	0.19077	0.00536	0.07779	0.00536	1125.6	29.0	1130.5	61.0	1141.5	172.8
16	0.19076	0.00770	2.00881	0.00087	0.07645	0.00752	1125.5	41.7	1118.5	63.8	1106.9	184.9
23	0.19007	0.00612	2.22350	0.00114	0.08469	0.00712	1121.8	33.2	1188.5	58.4	1308.4	154.9
2	0.18013	0.00766	2.41204	0.00081	0.09716	0.00881	1067.7	41.8	1246.2	60.4	1570.4	160.9
9	0.17942	0.00506	1.81366	0.00083	0.07343	0.00503	1063.8	27.7	1050.4	42.7	1025.9	132.6
5	0.17514	0.00495	1.78122	0.00078	0.07384	0.00488	1040.3	27.1	1038.6	40.6	1037.0	128.1
3	0.15851	0.00357	1.66696	0.00100	0.07632	0.00404	948.5	19.8	996.0	31.7	1103.5	102.3
35	1.54569	0.07373	0.15281	0.00239	0.07342	0.00239	916.7	13.4	948.8	29.4	1025.7	94.7
4	0.15069	0.00383	1.56797	0.00082	0.07553	0.00458	904.8	21.5	957.6	35.5	1082.6	117.0
29	0.15001	0.00490	1.70213	0.00107	0.08191	0.00734	901.0	27.5	1009.3	58.2	1243.4	166.2
12	0.13848	0.00336	1.34274	0.00107	0.07044	0.00431	836.1	19.1	864.4	34.2	941.1	120.5
39	1.43337	0.20932	0.12528	0.00491	0.08302	0.00491	760.9	28.2	903.0	87.3	1269.6	266.2
26	0.12184	0.00484	1.12034	0.00076	0.06648	0.00719	741.2	27.8	763.1	57.1	821.5	210.9
6	0.11741	0.00687	0.91179	0.00108	0.05641	0.00919	715.6	39.6	658.0	75.1	467.6	325.9
22	0.09140	0.00258	0.76164	0.00058	0.06035	0.00473	563.8	15.2	575.0	34.3	616.3	160.8
11	0.08908	0.00363	0.96494	0.00048	0.07869	0.00822	550.1	21.5	685.8	49.1	1164.5	194.1
32	0.70554	0.09115	0.08743	0.00262	0.05857	0.00262	540.3	15.6	542.1	54.3	551.3	264.1
25	0.08390	0.00418	0.73573	0.00076	0.06343	0.00948	519.4	24.8	559.9	62.5	722.7	288.8
34	0.54771	0.03128	0.06830	0.00115	0.05821	0.00115	425.9	6.9	443.5	20.5	537.1	122.9
10	0.03673	0.00221	0.25590	0.00024	0.05061	0.01065	232.5	13.7	231.4	41.9	223.1	425.1
40	0.16376	0.10117	0.02074	0.00132	0.05728	0.00132	132.3	8.4	154.0	88.3	501.8	982.4
19	0.01567	0.00179	0.10372	0.00025	0.04802	0.02354	100.2	11.3	100.2	45.6	99.0	874.6
27	0.01427	0.00191	0.10618	0.00022	0.05378	0.03759	91.3	12.1	102.5	67.0	361.9	1092.3
33	0.09256	0.01678	0.01397	0.00047	0.04809	0.00047	89.4	3.0	89.9	15.6	103.5	384.6
17	0.01183	0.00088	0.07776	0.00012	0.04771	0.01416	75.8	5.6	76.0	21.1	84.0	585.7
30	0.09413	0.02893	0.01041	0.00056	0.06564	0.00056	66.7	3.5	91.3	26.9	795.0	545.5
24	0.00927	0.00087	0.06214	0.00010	0.04851	0.01680	59.5	5.5	61.2	19.9	124.2	660.0
20	0.00910	0.00077	0.11849	0.00010	0.09449	0.02208	58.4	4.9	113.7	23.6	1518.0	386.4
38	0.05721	0.00743	0.00799	0.00020	0.05193	0.00020	51.3	1.3	56.5	7.1	282.3	275.3
15	0.00778	0.00052	0.05499	0.00005	0.05135	0.01135	49.9	3.3	54.4	11.2	256.6	441.6
36	0.13338	0.08419	0.00723	0.00081	0.13385	0.00081	46.5	5.2	127.1	75.4	2149.0	828.8
14	0.00705	0.00024	0.04889	0.00004	0.05037	0.00528	45.3	1.6	48.5	4.8	212.2	225.9

TABLE A5A. PETROGRAPHIC DATA

Site	Formation	Region	Sample	Grain size (μm)	Q	KF	P	Lv	Lc	Lp	Lch	Lm	M	HM	Total	MI
Corbyn's Cove section N11°38′43.0″ E92°45′29.2″	Andaman Flysch	S Andaman	FT1B	115	50	13	5	4	0	1	0	25	1	1	100.0	175
Corbyn's Cove section ~100 m upsection from 1A	Andaman Flysch	S Andaman	FT3	140	48	17	11	3	0	2	0	16	2	1	100.0	160
Corbyn's Cove section below hotel	Andaman Flysch	S Andaman	FT4	130	47	10	9	5	0	3	1	24	1	0	100.0	150
Namunagarh Quarry	Namunagarh Grit	S Andaman	NAM 3D	1500	2	1	41	52	0	0	0	1	0	2	100.0	2
Hopetown Quarry N11°41′40.7″ E92°43′50.1″	Namunagarh Grit	S Andaman	NAM 25A	850	21	2	27	40	0	2	2	5	0	1	100.0	15
Mungleton Quarry N11°34′22.3″ E92°39′54.1″	Namunagarh Grit	S Andaman	NAM 26	1800	19	1	30	45	0	1	1	3	0	0	100.0	11
Irrawaddy River ~ Nyaungdoun	Modern river sand	Myanmar	MY05 23A	—	47	11	11	6	0	6	1	15	2	1	100.0	112

Note: The MI ("Metamorphic Index"; Garzanti and Vezzoli, 2003) expresses the average rank of metamorphic rock fragments in the studied samples, and varies from 0 in detritus from sedimentary and volcanic cover rocks to 500 in detritus from high-grade basement rocks. Q—quartz; KF—potassium feldspar; P—plagioclase; Lv—volcanic; Lc—carbonate lithic fragments (including marble); Lp—terriginous lithic fragments (shale, siltstone); Lch—chert lithic fragments; Lm—metamorphic lithic fragments; M—micas; HM—heavy minerals.

TABLE A5B. HEAVY-MINERAL DATA

Site	Formation	Sample	HM% vfs–fs	HM% transparent	% transparent	% opaque	% turbid	Total	Zircon	Dravite	Schorlite	Rutile	Sagenite	Sphene
Corbyn's Cove section N11°38′43.0″ E92°45′29.2″	Andaman Flysch	FT1B	0.9	0.5	54	9	37	100	3	4	4	5	0	3
Corbyn's Cove section ~100 m upsection from 1A	Andaman Flysch	FT3	0.4	0.2	44	7	49	100	4	4	5	5	2	2
Corbyn's Cove section below hotel	Andaman Flysch	FT4	0.6	0.2	35	8	57	100	4	3	6	7	1	0
Namunagarh Quarry	Namunagarh Grit	NAM 3D	4.0	1.5	37	38	25	100	0	0	0	0	0	1
Hopetown Quarry N11°41′40.7″ E92°43′50.1″	Namunagarh Grit	NAM 25A	1.3	0.6	42	16	42	100	1	0	0	1	0	15
Mungleton Quarry N11°34′22.3″ E92°39′54.1″	Namunagarh Grit	NAM 26	1.0	0.5	53	7	40	100	0	0	0	1	0	16
Irrawaddy River ~ Nyaungdoun	River sand	MY05 23A	5.0	4.0	79	3	17	100	0	0	0	0	0	3

Site	Formation	Sample	Anatase	Brookite	Ti aggregates	Apatite	Xenotime	Monazite	Barite	Others	Blue-green hornblende	Green hornblende	Green-brown hornblende	Brown hornblende
Corbyn's Cove section N11°38′43.0″ E92°45′29.2″	Andaman Flysch	FT1B	0	0	24	10	0	0	0	0	0	0	0	0
Corbyn's Cove section ~100 m upsection from 1A	Andaman Flysch	FT3	0	0	30	17	0	1	0	0	0	0	0	0
Corbyn's Cove section below hotel	Andaman Flysch	FT4	0	0	24	11	0	0	0	0	0	0	0	0
Namunagarh Quarry	Namunagarh Grit	NAM 3D	0	0	0	3	0	0	0	0	1	2	20	0
Hopetown Quarry N11°41′40.7″ E92°43′50.1″	Namunagarh Grit	NAM 25A	0	0	3	1	0	0	0	0	0	0	0	0
Mungleton Quarry N11°34′22.3″ E92°39′54.1″	Namunagarh Grit	NAM 26	0	0	1	3	0	0	0	0	0	0	0	0
Irrawaddy River ~ Nyaungdoun	River sand	MY05 23A	0	0	0	0	0	0	0	0	44	2	2	1

(*continued*)

TABLE A5B. HEAVY-MINERAL DATA (*continued*)

Site	Formation	Sample	Oxyhornblende	Glaucophane	Sodic amphiboles	Tremolite	Actinolite	Antofillite	Other amphiboles	Hypersthene	Olivine	Spinel	Epidote	Clinozoisite
Corbyn's Cove section N11°38′43.0″ E92°45′29.2″	Andaman Flysch	FT1B	0	0	0	0	0	0	0	0	0	2	18	0
Corbyn's Cove section ~100 m upsection from 1A	Andaman Flysch	FT3	0	0	0	0	0	0	0	0	0	3	2	0
Corbyn's Cove section below hotel	Andaman Flysch	FT4	0	0	0	0	0	0	0	0	0	2	0	0
Namunagarh Quarry	Namunagarh Grit	NAM 3D	0	0	0	0	0	0	0	0	0	0	11	0
Hopetown Quarry N11°41′40.7″ E92°43′50.1″	Namunagarh Grit	NAM 25A	0	0	0	0	0	0	0	0	0	16	43	0
Mungleton Quarry N11°34′22.3″ E92°39′54.1″	Namunagarh Grit	NAM 26	0	0	0	0	0	0	0	0	0	7	44	0
Irrawaddy River ~ Nyaungdoun	River sand	MY05 23A	0	0	0	0	0	2	0	0	0	0	33	0

Site	Formation	Sample	Zoisite	Other epidotes	Prehnite	Pumpellyite	Chloritoid	Lawsonite	Carpholite	Garnet	Staurolite	Andalusite	Kyanite	Sillimanite	Total transparent
Corbyn's Cove section N11°38′43.0″ E92°45′29.2″	Andaman Flysch	FT1B	0	0	0	0	12	0	0	14	0	0	0	0	100
Corbyn's Cove section ~100 m upsection from 1A	Andaman Flysch	FT3	0	0	0	0	12	0	0	13	0	0	0	0	100
Corbyn's Cove section below hotel	Andaman Flysch	FT4	0	0	0	0	25	0	0	15	1	0	0	0	100
Namunagarh Quarry	Namunagarh Grit	NAM 3D	0	0	0	0	0	0	0	0	0	0	0	0	100
Hopetown Quarry N11°41′40.7″ E92°43′50.1″	Namunagarh Grit	NAM 25A	0	2	0	0	0	0	0	0	0	0	0	0	100
Mungleton Quarry N11°34′22.3″ E92°39′54.1″	Namunagarh Grit	NAM 26	0	0	0	0	0	0	0	1	0	0	0	0	100
Irrawaddy River ~ Nyaungdoun	River sand	MY05 23A	0	1	0	0	0	0	0	6	0	0	0	0	100

Note: HM—heavy minerals; vfs—very fine sand; fs—fine sand.

TABLE A6A. WHOLE ROCK Sm-Nd DATA

Sample	Location	Formation / GPS	Lithology	Sm	Nd	Sm/Nd	$^{147}Sm/^{144}Nd$	$^{143}Nd/^{144}Nd$	1σ (ppm)	εNd
Andaman Islands										
AN05-31	Namunagarh Quarry	Namunagarh Grit	Sandstone	4.83	25.3134	0.1909	0.1154	0.512271	16	–7.2
AN05 3E	Namunagarh Quarry	Namunagarh Grit	Mudstone	1.99	7.18860	0.2769	0.1674	0.512799	19	3.1
AF1A	Corbyn's Cove	Andaman Flysch	Mudstone	11.17	50.6900	0.2204	0.1332	0.512068	10	–11.1
AF2	Corbyn's Cove	Andaman Flysch	Sandstone	5.05	25.7129	0.1966	0.1188	0.512220	12	–8.2
Myanmar—Rivers draining Eocene rocks										
MY05 8A	Lemyu River	N20°49.212′, E93°18.576′	MR sand	4.02	20.0489	0.2010	0.1215	0.512300	18	–7.4
MY05 15A	Kyeintuli River	N17°57.139′, E94°33.087′	MR sand	3.33	16.4129	0.2035	0.1250	0.512434	14	–4.0
MY05 17B	Thanlwe River	N18°59.097′, E94°15.244′	MR mud	3.48	17.6156	0.1977	0.1195	0.512427	18	–4.1
MY05 22B	Thandwe River	N18°27.466′, E94°23.563′	MR mud	3.60	18.0331	0.1997	0.1207	0.512424	14	–4.2
MY05 23B	Irrawaddy River	N18°48.391′, E95°12.218′	MR mud	3.67	17.9317	0.2052	0.124	0.512210	18	–8.3

Note: MR—modern river sample; GPS—Global Positioning System.

TABLE A6B. SINGLE-GRAIN APATITE Sm-Nd DATA

Sample	Formation / Age	Lithology	$^{147}Sm/^{144}Nd$	2 S.D. of NIST610	2σ (internal)	$^{143}Nd/^{144}Nd$	2σ ppm	εNd (0)
1	Andaman Flysch AF1A Corbyn's Cove	Apatite grain	0.123272	0.001140	0.000069	0.512855	134	4.24
2	Andaman Flysch AF1A Corbyn's Cove	Apatite grain	0.070462	0.000408	0.000065	0.512803	127	3.21
3	Andaman Flysch AF1A Corbyn's Cove	Apatite grain	0.090724	0.000581	0.000058	0.512237	114	–7.83
4	Andaman Flysch AF1A Corbyn's Cove	Apatite grain	0.073481	0.000171	0.000054	0.512588	105	–0.98
5	Andaman Flysch AF1A Corbyn's Cove	Apatite grain	0.082561	0.000180	0.000031	0.512485	61	–2.98
6	Andaman Flysch AF1A Corbyn's Cove	Apatite grain	0.100785	0.002208	0.000062	0.512404	121	–4.57
7	Andaman Flysch AF1A Corbyn's Cove	Apatite grain	0.106736	0.000552	0.000046	0.512211	90	–8.33
8	Andaman Flysch AF1A Corbyn's Cove	Apatite grain	0.093898	0.000488	0.000033	0.511800	65	–16.35
9	Andaman Flysch AF1A Corbyn's Cove	Apatite grain	0.108342	0.001112	0.000047	0.512545	93	–1.81
10	Andaman Flysch AF1A Corbyn's Cove	Apatite grain	0.099159	0.000388	0.000033	0.512669	64	0.61
11	Andaman Flysch AF1A Corbyn's Cove	Apatite grain	0.113837	0.000346	0.000051	0.512794	99	3.03
12	Andaman Flysch AF1A Corbyn's Cove	Apatite grain	0.120108	0.000750	0.000044	0.512621	86	–0.33
13	Andaman Flysch AF1A Corbyn's Cove	Apatite grain	0.078972	0.000114	0.000067	0.512291	131	–6.77
14	Andaman Flysch AF1A Corbyn's Cove	Apatite grain	0.067596	0.000236	0.000075	0.512425	147	–4.16
15	Andaman Flysch AF1A Corbyn's Cove	Apatite grain	0.114968	0.000317	0.000043	0.511822	83	–15.92
16	Andaman Flysch AF1A Corbyn's Cove	Apatite grain	0.105069	0.001427	0.000067	0.512792	131	3.01
17	Andaman Flysch AF1A Corbyn's Cove	Apatite grain	0.117803	0.000238	0.000055	0.512607	108	–0.60
18	Andaman Flysch AF1A Corbyn's Cove	Apatite grain	0.085210	0.000165	0.000056	0.512321	109	–6.19
19	Andaman Flysch AF1A Corbyn's Cove	Apatite grain	0.102799	0.000424	0.000051	0.512782	99	2.80
20	Andaman Flysch AF1A Corbyn's Cove	Apatite grain	0.082935	0.000202	0.000136	0.512486	266	–2.96
21	Andaman Flysch AF1A Corbyn's Cove	Apatite grain	0.136207	0.000550	0.000118	0.512192	230	–8.71
22	Andaman Flysch AF1A Corbyn's Cove	Apatite grain	0.131323	0.000741	0.000062	0.512791	122	2.99
23	Andaman Flysch AF1A Corbyn's Cove	Apatite grain	0.244791	0.003438	0.000076	0.512607	148	–0.61
24	Andaman Flysch AF1A Corbyn's Cove	Apatite grain	0.172124	0.000850	0.000079	0.512771	154	2.59

Note: Global Positioning System (GPS) reference for AF1A Corbyn's Cove: N11°38.430' E92°45.292'; S.D.—standard deviation.

ACKNOWLEDGMENTS

This paper has benefited from thoughtful reviews by Peter Clift, Joseph Curray, and Christophe Colin. The work was funded by NERC grants NE/B503192/1 and NER/S/A/2004/12158, with additional support from the Royal Society short-visits scheme.

REFERENCES CITED

Acharyya, S.K., Ray, K.K., and Roy, D.K., 1989, Tectonic stratigraphy and emplacement history of the ophiolite assemblage from Naga Hills and Andaman island arc, India: Journal of the Geological Society of India, v. 33, p. 4–18.

Ahmad, T., Harris, N., Bickle, M., Chapman, H., Bunbury, J., and Prince, C., 2000, Isotopic constraints on the structural relationships between the Lesser Himalayan Series and the High Himalayan Crystalline Series, Garhwal Himalaya: Geological Society of America Bulletin, v. 112, p. 467–477, doi: 10.1130/0016-7606(2000)112<0467:ICOTSR>2.3.CO;2.

Auge, T., Cocherie, A., Genna, A., Armstrong, R., Guerrot, C., Mukherjee, N.M., and Patra, R.N., 2003, Age of the Baula PGE mineralization (Orissam India) and its implications concerning the Singhbhum Archaean nucleus: Precambrian Research, v. 121, p. 85–101, doi: 10.1016/S0301-9268(02)00202-4.

Bandopadhyay, P.C., 2005, Discovery of abundant pyroclasts in Namunagarh Grit, South Andaman; evidence for arc volcanism and active subduction during the Palaeogene in the Andaman area: Journal of Asian Earth Sciences, v. 25, p. 95–107, doi: 10.1016/j.jseaes.2004.01.007.

Bandopadhyay, P.C., and Ghosh, M., 1999, Facies, petrology and depositional environment of the Tertiary sedimentary rocks around Port Blair, South Andaman: Journal of the Geological Society of India, v. 52, p. 53–66.

Barley, M.E., Pickard, A.L., Zaw, K., Rak, P., and Doyle, M.G., 2003, Jurassic to Miocene magmatism and metamorphism in the Mogok metamorphic belt and the India-Eurasia collision in Myanmar: Tectonics, v. 22, p. 1019, doi: 10.1029/2002TC001398.

Bertrand, G., Rangin, C., Maluski, H., Han, T.A., Thein, M., Myint, O., Maw, W., and Lwin, S., 1999, Cenozoic metamorphism along the Shan scarp (Myanmar): Evidences for ductile shear along the Sagaing fault or the northward migration of the eastern Himalayan syntaxis?: Geophysical Research Letters, v. 26, p. 915–918, doi: 10.1029/1999GL900136.

Bertrand, G., Rangin, C., Maluski, H., and Bellon, H., 2001, Diachronous cooling along the Mogok Metamorphic Belt (Shan scarp, Myanmar): The trace of the northward migration of the Indian syntaxis: Journal of Asian Earth Sciences, v. 19, p. 649–659, doi: 10.1016/S1367-9120(00)00061-4.

Bodet, F., and Schärer, U., 2000, Evolution of the SE-Asian continent from U-Pb and Hf isotopes in single grains of zircon and baddeleyite from large rivers: Geochimica et Cosmochimica Acta, v. 64, p. 2067–2209, doi: 10.1016/S0016-7037(00)00352-5.

Brewer, I.D., Burbank, D.W., and Hodges, K.V., 2003, Modelling detrital cooling-age populations: Insights from two Himalayan catchments: Basin Research, v. 15, p. 305–320, doi: 10.1046/j.1365-2117.2003.00211.x.

Campbell, I.H., Reiners, P.W., Allen, C.M., Nicolescu, S., and Upadhyay, R., 2005, He-Pb double dating of detrital zircons from the Ganges and Indus Rivers: Implication for quantifying sediment recycling and provenance studies: Earth and Planetary Science Letters, v. 237, p. 402–432, doi: 10.1016/j.epsl.2005.06.043.

Carter, A., 1999, Present status and future avenues of source region discrimination and characterization using fission-track analysis: Sedimentary Geology, v. 124, p. 31–45, doi: 10.1016/S0037-0738(98)00119-5.

Carter, A., and Bristow, C.S., 2000, Detrital zircon geochronology: Enhancing the quality of sedimentary source information through improved methodology and combined U-Pb and fission track techniques: Basin Research, v. 12, p. 47–57, doi: 10.1046/j.1365-2117.2000.00112.x.

Chakraborty, P.P., and Pal, T., 2001, Anatomy of a forearc submarine fan: Upper Eocene–Oligocene Andaman Flysch Group, Andaman Islands, India: Gondwana Research, v. 4, p. 477–487, doi: 10.1016/S1342-937X(05)70347-6.

Chakraborty, P.P., Pal, T., Dutta Gupta, T., and Gupta, K.S., 1999, Facies pattern and depositional motif in an immature trench-slope basin, Eocene Mithakhari Group, Middle Andaman, India: Journal of the Geological Society of India, v. 53, p. 271–284.

Charusiri, P., Clark, A.H., Farrar, E., Archibald, D., and Charusiri, B., 1993, Granite belts in Thailand: Evidence from the $^{40}Ar/^{39}Ar$ geochronological and geological syntheses: Journal of Southeast Asian Earth Sciences, v. 8, p. 127–136, doi: 10.1016/0743-9547(93)90014-G.

Cherniak, D.J., and Watson, E.B., 2001, Pb diffusion in zircon: Chemical Geology, v. 172, p. 5–24, doi: 10.1016/S0009-2541(00)00233-3.

Clark, M.K., Schoenbohm, L.M., Royden, L., Whipple, K.X., Burchfiel, B.C., Zhang, X., Tang, W., Wang, E., and Chen, L., 2004, Surface uplift, tectonics, and erosion of eastern Tibet from large-scale drainage patterns: Tectonics, v. 23, p. TC1006, doi: 10.1029/2002TC001402.

Clark, M.K., House, M.A., Royden, L.H., Whipple, K.X., Burchfiel, B.C., Zhang, X., and Tang, W., 2005, Late Cenozoic uplift of southeastern Tibet: Geology, v. 33, p. 525–528, doi: 10.1130/G21265.1.

Colin, C., Turpin, L., Bertaux, J., Desprairies, A., and Kissel, C., 1999, Erosional history of the Himalayan and Burman ranges during the last two glacial-interglacial cycles: Earth and Planetary Science Letters, v. 171, p. 647–660, doi: 10.1016/S0012-821X(99)00184-3.

Colin, C., Turpin, L., Bertaux, J., Frank, N., Kissel, C., and Duchamp, S., 2006, Evolution of weathering patterns in the Indo-Burman Ranges over the last 280 kyr: Effects of sediment provenance on $^{87}Sr/^{86}Sr$ ratios tracer: Geochemistry, Geophysics, Geosystems, v. 7, p. 1–16, doi:10.1029/2005GC000962.

Curray, J.R., 2005, Tectonics and history of the Andaman Sea region: Journal of Asian Earth Sciences, v. 25, p. 187–232, doi: 10.1016/j.jseaes.2004.09.001.

Curray, J.R., Moore, D.G., Lawver, L.A., Emmel, F.J., Raitt, R.W., Henry, M., and Kieckhefer, R., 1979, Tectonics of the Andaman Sea and Burma, *in* Watkins, J., et al., eds., Geological and Geophysical Investigations of Continental Margins: American Association of Petroleum Geologists Memoir 29, p. 189–198.

DeCelles, P.G., Gehrels, G.E., Quade, J., and Ojha, T.P., 1998, Eocene to early Miocene foreland basin development and the history of Himalayan thrusting, western and central Nepal: Tectonics, v. 17, p. 741–765, doi: 10.1029/98TC02598.

DeCelles, P.G., Gehrels, G.E., Najman, Y., Martin, A.J., and Garzanti, E., 2004, Detrital geochronology and geochemistry of Cretaceous–Early Miocene strata of Nepal: Implications for timing and diachroneity of initial Himalayan orogenesis: Earth and Planetary Science Letters, v. 227, p. 313–330, doi: 10.1016/j.epsl.2004.08.019.

Dickinson, W.R., 1985, Interpreting provenance relations from detrital modes of sandstones: Provenance of arenites, *in* Zuffa, G.G., ed., NATO ASI: Dordrecht, Netherlands, Reidel, v. 148, p. 333–361.

Draut, A.E., and Clift, P.D., 2006, Sedimentary processes in modern and ancient oceanic arc settings: Evidence from the Jurassic Talkeetna Formation of Alaska and the Mariana and Tonga Arcs, western Pacific: Journal of Sedimentary Research, v. 76, p. 493–514, doi: 10.2110/jsr.2006.044.

Foster, G.L., and Vance, D., 2006, In situ Nd isotopic analysis of geological materials by laser ablation MC-ICP-MS: Journal of Analytical Atomic Spectrometry, v. 21, p. 288–296, doi: 10.1039/b513945g.

Galbraith, R.F., and Green, P.F., 1990, Estimating the component ages in a finite mixture: Nuclear Tracks and Radiation Measurements, v. 17, p. 197–206, doi: 10.1016/1359-0189(90)90035-V.

Galbraith, R.F., and Laslett, G.M., 1993, Statistical models for mixed fission track ages: Nuclear Tracks and Radiation Measurements, v. 21, p. 459–470, doi: 10.1016/1359-0189(93)90185-C.

Gallagher, K., 1995, Evolving temperature histories from apatite FT data: Earth and Planetary Science Letters, v. 136, p. 421–435, doi: 10.1016/0012-821X(95)00197-K.

Galy, A., and France-Lanord, C., 2001, Higher erosion rates in the Himalaya: Geochemical constraints on riverine fluxes: Geology, v. 29, p. 23–26, doi: 10.1130/0091-7613(2001)029<0023:HERITH>2.0.CO;2.

Garzanti, E., and Vezzoli, G., 2003, A classification of metamorphic grade in sands based on their composition and grade: Journal of Sedimentary Research, v. 73, p. 830–837.

Green, P.F., Duddy, I.R., and Bray, R.J., 1995, Applications of thermal history reconstruction in inverted basins, *in* Buchanan, J.G., and Buchanan, P.G., eds., Basin Inversion: Geological Society [London] Special Publication 88, p. 149–165.

Guha, D.K., and Mohan, M., 1965, On the ostracod from the Neogene of Andaman Island: Journal of the Geological Survey of India, v. 9, p. 58–66.

Guillot, S., Garzanti, E., Baratoux, D., Marquer, D., Mahéo, G., and de Sigoyer, J., 2003, Reconstructing the total shortening history of the NW Himalaya: Geochemistry, Geophysics, Geosystems, v. 4, p. 1064, doi: 10.1029/2002GC000484.

Haines, P.W., Turner, S.P., Kelley, S.P., Wartho, J.-A., and Sherlock, S.C., 2004, Ar/Ar dating of detrital muscovite in provenance investigations: A case study from the Adelaide Rift Complex, South Australia: Earth and Planetary Science Letters, v. 227, p. 297–311, doi: 10.1016/j.epsl.2004.08.020.

Halder, D., 1985, Some aspects of the Andaman Ophiolite Complex: Geological Survey of India, v. 115, p. 1–11.

Hurford, A.J., 1990, Standardization of fission track dating calibration: Recommendation by the Fission Track Working Group of the IUGS Subcommission on Geochronology: Chemical Geology, v. 80, p. 177–178.

Karunakaran, C., Ray, K.K., and Saha, S.S., 1968, Tertiary sedimentation in Andaman-Nicobar geosyncline: Journal of the Geological Society of India, v. 9, p. 32–39.

Ketcham, R.A., Donelick, R.A., and Carlson, W.D., 1999, Variability of apatite fission-track annealing kinetics: III. Extrapolation to geological timescales: American Mineralogist, v. 84, p. 1235–1255.

Khan, P.K., and Chakraborty, P.P., 2005, Two-phase opening of Andaman Sea: A new seismotectonic insight: Earth and Planetary Science Letters, v. 229, p. 259–271.

Lee, T.T., and Lawver, L.A., 1995, Cenozoic plate reconstruction of Southeast Asia: Tectonophysics, v. 251, p. 85–138, doi: 10.1016/0040-1951(95)00023-2.

Mallik, T.K., 1976, Shelf sediments of the Ganges delta with special emphasis on the mineralogy of the western part, Bay of Bengal, Indian Ocean: Marine Geology, v. 22, p. 1–32, doi: 10.1016/0025-3227(76)90007-4.

Marsaglia, K.M., and Ingersoll, R.V., 1992, Compositional trends in arc-related, deep-marine sand and sandstone; a reassessment of magmatic-arc provenance: Geological Society of America Bulletin, v. 104, p. 1637–1649, doi: 10.1130/0016-7606(1992)104<1637:CTIARD>2.3.CO;2.

Meesters, A.G.C.A., and Dunai, T.J., 2002, Solving the production diffusion equation for finite diffusion domains of various shapes; Part II, Application to cases with alpha-ejection and nonhomogeneous distribution of the source: Chemical Geology, v. 186, p. 57–73, doi: 10.1016/S0009-2541(01)00423-5.

Metcalfe, I., 1996, Pre-Cretaceous evolution of SE Asian terranes, *in* Hall, R., and Blundell, D., eds., Tectonic Evolution of Southeast Asia: Geological Society [London] Special Publication 106, p. 97–122.

Mishra, M., and Rajamani, V., 1999, Significance of the Archaean bimodal volcanics from the Ramagiri schist belt in the formation of the Eastern Dharwar craton: Journal of the Geological Society of India, v. 54, p. 563–583.

Mitchell, A.H.G., 1993, Cretaceous–Cenozoic tectonic events in the western Myanmar (Burma)–Assam region: Geological Society [London] Journal, v. 150, p. 1089–1102.

Mountain, G.S., and Prell, W.L., 1990, A multiphase plate tectonic history of the southeast continental margin of Oman, *in* Robertson, A.H.F., et al., eds., The Geology and Tectonics of the Oman Region: Geological Society [London] Special Publication 49, p. 725–743.

Najman, Y., and Garzanti, E., 2000, Reconstructing early Himalayan tectonic evolution and paleogeography from Tertiary foreland basin sedimentary rocks, northern India: Geological Society of America Bulletin, v. 112, p. 435–449, doi: 10.1130/0016-7606(2000)112<0435:REHTEA>2.3.CO;2.

Najman, Y., Bickle, M., and Chapman, H., 2000, Early Himalayan exhumation: Isotopic constraints from the Indian foreland basin: Terra Nova, v. 12, p. 28–34, doi: 10.1046/j.1365-3121.2000.00268.x.

Najman, Y., Johnson, C., White, N.M., and Oliver, G., 2004, Evolution of the Himalayan foreland basin, NW India: Basin Research, v. 16, p. 1–24, doi: 10.1111/j.1365-2117.2004.00223.x.

Najman, Y., Carter, A., Oliver, G., and Garzanti, E., 2005, Provenance of early foreland basin sediments, Nepal: Constraints to the timing and diachroneity of early Himalayan orogenesis: Geology, v. 33, p. 309–312, doi: 10.1130/G21161.1.

Oldham, R.D., 1885, Notes on the geology of Andaman Islands: Record of the Geological Survey of India. v. 18, p. 135–145.

Pal, T., Chakraborty, P.P., Gupta, T.D., and Singh, C.D., 2003, Geodynamic evolution of the outer-arc–forearc belt in the Andaman Islands, the central part of the Burma-Java subduction complex: Geological Magazine, v. 140, p. 289–307, doi: 10.1017/S0016756803007805.

Pal, T., Gupta, T.D., Chakraborty, P.P., and Gupta, S.C.D., 2005, Pyroclastic deposits of Mio-Pliocene age in the Arakan Yoma-Andaman-Java subduction complex, Andaman Islands, Bay of Bengal, India: Geochemical Journal, v. 39, p. 69–82, doi: 10.2343/geochemj.39.69.

Peucat, J.J., Vidal, P., Bernard-Griffiths, J., and Condie, K.C., 1989, Sr, Nd and Pb isotopic systematics in the Archaean low-to-high-grade transition zone of southern India: Syn-accretion granulites: Journal of Geology, v. 97, p. 537–550.

Pivnik, D.A., Nahm, J., Tucker, R.S., Smith, G.O., Nyein, K., Nyunt, M., and Maung, P.H., 1998, Polyphase deformation in a fore-arc/back-arc basin, Salin sub-basin, Myanmar (Burma): American Association of Petroleum Geologists Bulletin, v. 82, p. 1837–1856.

Ray, K.K., Sengupta, S., and Van Den Hul, H.J., 1988, Chemical characters of volcanic rocks from Andaman ophiolite, India: Geological Society [London] Journal, v. 145, p. 392–400.

Renne, P.R., Swisher, C.C., Deino, A.L., Karner, D.B., Owens, T.L., and DePaolo, D.J., 1998, Intercalibration of standards, absolute ages and uncertainties in $^{40}Ar/^{39}Ar$ dating: Chemical Geology, v. 145, p. 117–152, doi: 10.1016/S0009-2541(97)00159-9.

Robinson, D.M., DeCelles, P.G., Patchett, P.J., and Garzione, C.N., 2001, The kinematic evolution of the Nepalese Himalaya interpreted from Nd isotopes: Earth and Planetary Science Letters, v. 192, p. 507–521, doi: 10.1016/S0012-821X(01)00451-4.

Rowley, D.B., 1996, Age of initiation of collision between India and Asia: A review of stratigraphic data: Earth and Planetary Science Letters, v. 145, p. 1–13, doi: 10.1016/S0012-821X(96)00201-4.

Roy, S.K., 1992, Accretionary prism in Andaman forearc: Geological Survey of India Special Publication 29, p. 273–278.

Roy, T.K., 1983, Geology and hydrocarbon prospects of Andaman–Nicobar basin, *in* Bhandari, L.L., ed., Petroliferous Basins of India: Petroleum Asia Journal, p. 37–50.

Saha, A., Basu, A.R., Garzione, C.N., Bandyopadhyay, P.K., and Chakrabarti, A., 2004, Geochemical and petrological evidence for subduction-accretion processes in the Archean Eastern Indian Craton: Earth and Planetary Science Letters, v. 220, p. 91–106, doi: 10.1016/S0012-821X(04)00056-1.

Sambridge, M.S., and Compston, W., 1994, Mixture modelling of multi-component data sets with application to ion-probe zircons: Earth and Planetary Science Letters, v. 128, p. 373–390, doi: 10.1016/0012-821X(94)90157-0.

Sherlock, S.C., and Kelley, S.P., 2002, Excess argon in HP-LT rocks: A UV laserprobe study of phengite and K-free minerals: Chemical Geology, v. 182, p. 619–636, doi: 10.1016/S0009-2541(01)00345-X.

Singh, O.P., Subramanya, S.M., and Sharma, V., 2000, Early Neogene multiple microfossil biostratigraphy, John Lawrence Island: Andaman Sea: Micropalaeontology, v. 46, p. 343–352.

Singh, S.K., and France-Lanord, C., 2002, Tracing the distribution of erosion in the Brahmaputra watershed from isotopic compositions of stream sediments: Earth and Planetary Science Letters, v. 202, p. 645–662, doi: 10.1016/S0012-821X(02)00822-1.

Svojtka, M., Ko, J., and Venera, Z., 2001, Dating granulite-facies structures and the exhumation of lower crust in the Moldanubian Zone of the Bohemian Massif: International Journal of Earth Sciences, v. 91, p. 373–385.

MANUSCRIPT ACCEPTED BY THE SOCIETY 24 APRIL 2007